Collective excitations of quasi-two-dimensional trapped dipolar fermions: Transition from collisionless to hydrodynamic regime

Mehrtash Babadi and Eugene Demler
Physics Department, Harvard University, Cambridge, Massachusetts 02138, USA
(Received 5 October 2012; published 28 December 2012)

We study the collective excitations of polarized single-component quasi-two-dimensional dipolar fermions in an isotropic harmonic trap by solving the collisional Boltzmann-Vlasov (CBV) equation via the method of moments. We study the response to monopole and quadrupole perturbations of the trap potential and investigate the dynamical character of excitations in each case. Simple analytic formulas are found using the linearized scaling ansatz approximation and accurate numerical results are obtained by satisfying the first eight moments of the CBV equation. Except for the lowest-lying monopole mode that is weakly affected by collisions, the quadrupole and the higher-order monopole modes undergo a transition from the collisionless regime to a dissipative crossover regime and finally approach the hydrodynamic regime upon increasing the dipolar interaction strength. For strong transverse confinement (2D limit), we predict the existence of a temperature window within which the characteristics of the collective modes become temperature independent. This plateau, which is a direct consequence of dipole-dipole scatterings, persists as long as the scattering energies remain in the near-threshold regime. The predictions of this work are expected to be observable in the current experiments.

DOI: 10.1103/PhysRevA.86.063638 PACS number(s): 03.75.Ss, 67.85.Lm, 67.10.Jn

I. INTRODUCTION

Dipolar quantum gases have been the subject of much interest and significant experimental and theoretical investigations in the recent years. The long-range anisotropic dipole-dipole interactions give rise to novel phenomena and applications in these systems (see Ref. [1] and references therein). Dipolar Bose-Einstein condensates (BECs) with magnetic dipole-dipole interactions have been exhaustively studied both theoretically and experimentally [2]. The most recent experimental achievements along this line are the realization of BECs of rare-earth atoms such as ^{164}Dy [3] and ^{168}Er [4] with large magnetic dipole moments of $10\mu_B$ and $7\mu_B$, respectively. The many-body effects of dipolar interactions are much easier to observe in dipolar BECs compared to dipolar Fermi gases. Pauli exclusion sets a large energy scale set for fermions and stronger dipolar interactions are required for the interaction effects to become appreciable.

Since electric dipole-dipole interactions are typically stronger than magnetic ones, much of the recent experimental efforts have been focused on the realization of ultracold heternucleus bialkali molecules which have large permanent electric dipole moments. An important experimental achievement in this direction was the realization of a nearly quantum degenerate gas of fermionic KRb molecules at JILA [5]. Unfortunately, complexities arising from ultracold chemistry results in significant molecule loss and have also hampered further evaporative cooling to quantum degeneracy. The experiments with other bialkali fermionic polar molecules such as LiCs [6,7] are also making significant progress.

More recently, the group at Stanford has realized a quantum degenerate gas of fermionic ^{161}Dy through sympathetic cooling with the bosonic species ^{162}Dy [8]. Having a large permanent magnetic dipole moment of $10\mu_B$ and being free of the complication of ultracold chemistry, these species have brought a new hope toward the experimental observation of many-body dipolar physics.

An important experimental probe for the many-body physics of ultracold gases is the measurement of collective oscillations of trapped gases in response to perturbations of the trap potential. These oscillations constitute the low-lying collective excitations of these systems. The measurement of the frequency and damping of these oscillations can be utilized to understand the properties of the ground state and to extract important information such as the character of self-energy corrections, the equilibrium equation of state, and the kinetic coefficients. Moreover, the possibility of carrying out extremely precise measurements of these quantities allows us to put our theoretical understanding of the system to the test. For instance, by measuring the frequency of the radial breathing mode for a two-component Fermi gas near the BEC-BCS crossover with a 10^{-3} accuracy level, the Innsbruck group could clearly verify the quantum Monte Carlo result for the unitary gas and invalidate the predictions of the BCS theory [9]. Another remarkable example is the recent measurement of the universal quantum viscosity of the unitary gas [10] that confirmed the theoretical $T^{3/2}$ scaling and also provided evidence for a conjecture on the lower bound for the viscosity/entropy ratio obtained using string-theory methods [11]. At the moment, the collective oscillations of trapped BECs [12] and two-component atomic gases with s-wave interactions in three dimensions [13] are both understood fairly well. Recently, the experimental and theoretical studies of the 2D Fermi gas interacting via s-wave Feshbach resonances have also shown remarkable progress [14–18].

In this paper, we study the collective modes of quasi-two-dimensional (quasi-2D) dipolar fermionic gases prepared in a single hyperfine state and loaded into an isotropic harmonic trap. Experimentally, this configuration may be realized using a highly anisotropic optical dipole trap such that $\omega_z \gg \omega_x = \omega_y$, where ω_i is the trap frequency along ith axis. Stronger transverse confinements (larger ω_z) can be achieved using an optical lattice to slice the trapped gas into thin "pancakes" [5]. In that case, we confine our attention

to a single pancake here. We assume that the dipoles are aligned perpendicular to the confining plane (see Fig. 2). In this setting, the effective dipole-dipole interactions have a repulsive long-range character and give rise to a normal Fermi liquid state. This particular configuration is also necessary in order to suppress inelastic dipolar collisions and also to reduce the rate of chemical reactions in experiments with reactive bialkali polar molecules.

In highly quantum degenerate Fermi liquids ($T \ll T_F$, where T_F is the Fermi temperature), the elastic collisions are suppressed due to Pauli exclusion and collisional effects may be ignored as a first approximation in the study of collective excitations. In this so-called collisionless (CL) limit, the collective modes are undamped and no energy dissipation occurs. As the temperature is increased, the collision rate rapidly grows and the collisional effects may no longer be ignored. In this regime, the dynamics is dissipative and the collective modes are damped. However, if the collision rate surpasses the typical frequency of collective oscillations (whose scale is set by the trap frequency), the gas will remain "locally" in a thermal equilibrium and a hydrodynamical (HD) description emerges [19]. This ideal HD limit is again dissipationless and the quasiequilibrium dynamics is simply described by differential conservation laws of mass, momentum, and energy currents [19,20]. A realistic system, however, typically lies in the dissipative "crossover" regime between these two ideal limits [21]. An important aspect of understanding a many-body system is to determine where it lies within the CL-HD spectrum, both qualitatively and quantitatively.

The theoretical investigation of collective modes of trapped dipolar fermions has started more than a decade ago. Góral *et al.* have studied the stability condition [22] and HD excitations in traps with different degrees of of anisotropy [23] at zero temperature. Lima *et al.* have studied the same problems in more detail [24,25], while Sogo *et al.* have studied the the CL limit [26]. More recently, Abad *et al.* have compared the predictions of CL and HD formulations at zero temperature for vertically aligned and tilted dipoles [27].

In light of the recent experimental progress with dipolar fermions and the possibility of carrying out precise measurement of the collective modes, it is worthwhile to carry out a more detailed and quantitatively reliable theoretical treatment of this problem. The issue of finite temperature has not been addressed in any of the above works and once the thermal effects are taken into account, all of the previously used formulations become unreliable. The applicability of ideal HD formulation at zero temperature is questionable since collisions are absent. Also, the CL approximation is only relevant to extremely quantum degenerate conditions which is not within the reach of the experiments yet. Most importantly, the crossover regime, which is most relevant to current experiments, has not been studied so far.

Here, we make no prior assumption about where the system lies in the CL-HD spectrum. We use the framework of quantum kinetic equations (in particular, the collisional Boltzmann-Vlasov limit), which, in principle, allows us to study the dynamics in the whole spectrum in a unified way. The CL and HD limits emerge naturally when the right physical conditions are met. We evaluate the linear response of the gas to monopole and quadrupole perturbations of the trap potential and study the oscillation frequency and damping of the generated excitations. We restrict our analysis to situations where collisions lie well within the near-threshold scattering regime so that Born approximation is applicable [28,29]. This condition is satisfied well in the current experiments.

We carry out the calculations in two stages. First, we neglect the self-energy corrections to quasiparticle dispersions (the Boltzmann limit) and utilize the widely used linearized scaling ansatz approximation [30] to obtain a simple semianalytic picture. In the second stage, we include the self-energy corrections to quasiparticle dispersions and also extend the scaling ansatz by including higher-order moments (up to the eighth order). We find that both of these refinements result in significant quantitative corrections. Furthermore, inclusion of higher moments allows us to study higher-order modes in addition to the nodeless modes described by the scaling ansatz.

Before delving into the formalism and details, we find it useful to briefly summarize our main results, some of which are unique features of dipolar fermions in 2D. Without self-energy corrections, the scaling ansatz analysis predicts the well-known undamped monopole oscillations at a fixed frequency of $2\omega_0$, independent of the interaction strength and temperature [31,32]. Here, $\omega_0 \equiv \omega_x = \omega_y$ is the in-plane trap frequency. Taking self-energy corrections into account, we find that the oscillation frequency of the nodeless monopole mode increases from $2\omega_0$ due to the repulsive interactions while it also assumes a small damping (see Fig. 6). While collisions have a small influence on the dynamics of the scaling mode, we find that higher-order monopole modes are strongly influenced by collisions: They go through a dissipative crossover regime as the interaction strength is increased and finally approach the HD regime (see Fig. 1).

The quadrupole modes, including the lowest-lying nodeless mode, exhibit the same CL-to-HD transition. In particular, the oscillation frequency of the nodeless quadrupole mode approaches $\sqrt{2}\omega_0$ in the collision-dominated regime, which is the universal frequency of the quadrupole "surface" mode [33] (see Fig. 9). The appearance of surface modes is an indication for the emergence of hydrodynamics.

We find simple analytic results in the Boltzmann limit using the linearized scaling ansatz approximation. In particular, we find that the frequency and damping of the quadrupole oscillations are controlled by a single parameter, the quadrupole collision rate ν_c (see Sec. V B). Small and large values of ν_c correspond to CL and HD behavior, respectively. For small T/T_F, we obtain $\nu_c \sim T^2$, which is due to Pauli blocking. For large T/T_F, the behavior of ν_c depends on the degree of quasi-two-dimensionality ([quantified by η; see Eq. (13)]. In the strictly 2D limit, we show that ν_c reaches a plateau for $T \gtrsim T_F$. The existence of this plateau is a unique feature of 2D dipolar fermions and results from the balance between rarefaction of the gas at higher temperatures and the growth of the dipolar scattering cross section. The high-temperature cutoff for this plateau behavior is $T_{\rm dip} \equiv \hbar^2/(m a_d^2 k_B)$, where $a_d \equiv m D^2/\hbar^2$ is the "dipolar length." Here, m and D denote the mass and the dipole moment of a single particle. For $T \gtrsim T_{\rm dip}$, the scattering energies become semiclassical and we find $\nu_c \sim T^{-3/4}$.

Figure 1 shows a qualitative comparison between the behavior of quadrupole oscillations in 2D two-component

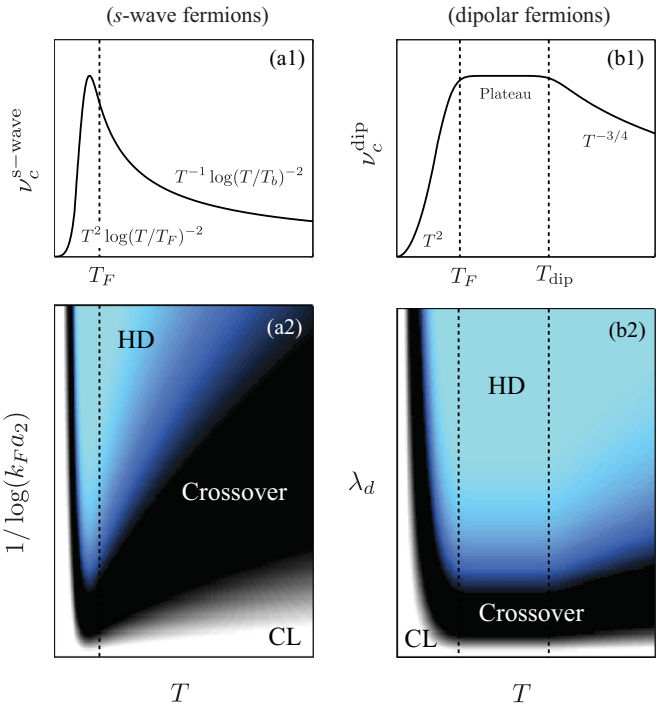

FIG. 1. (Color online) Qualitative comparison between the dynamical regimes of quadrupole oscillations of 2D s-wave and dipolar fermions in harmonic traps. Panels (a1) and (b1) show the temperature dependence of the collision rates of s-wave and dipolar fermions respectively. Panels (a2) and (b2) show the resulting dynamical regimes as a function of interaction strength and temperature. The asymptotics of $\nu_c^{s-\rm wave}$ is due to [15]. k_F is the trap Fermi momentum, a_2 is the 2D scattering length and $T_b = \hbar^2/(mk_B a_2^2)$. See Eqs. (13) and (25) for the definition of the parameters appearing in (b1) and (b2). Please refer to the main text for details.

fermions interacting via a s-wave Feshbach resonance (simply, s-wave fermions) and 2D dipolar fermions. The top and bottom panels show the temperature dependence of ν_c and the resulting dynamical regimes of quadrupole oscillations as a function of interaction parameter and temperature. The discussed regimes of ν_c for 2D dipolar fermions can be seen in panel (b1). It is worthy of mention that the temperature window in which ν_c is appreciably large is "universal" for 2D s-wave fermions. For 2D dipolar fermions, however, this window is amenable to experimental tuning (see Sec. VIII).

We look into the effect of mean-field correction to quasiparticle dispersions and show that it has a significant effect in the quantum degenerate regime. This is again in contrast to the case of s-wave fermions where self-energy correction is found to have a small effect on the frequency of collective modes [34]. Finally, going beyond the scaling ansatz by satisfying higher-order moments of the CBV equation, we show that the simple scaling ansatz overestimates the collision rates, in agreement with the findings of Ref. [35]. We also show that refinements to the predictions for the lowest-lying monopole and quadrupole modes become negligible beyond fourth-order moments. Finally, we discuss the observability of our predictions in the experiments with ^{40}K-^{87}Rb and ^{161}Dy and show that although the HD regime is not currently achievable, a significant collisional damping and the plateau in the collision rates are both expected to be observable.

This paper is organized as follows. In Sec. II, we describe the model in detail and define the response functions. A brief overview of the quantum kinetic equations, the approximations leading to the CBV equation, and their validity conditions, are given in Sec. II C. We discuss the equilibrium state of the trapped gas in Sec. III. The linear response theory of the CBV equation is described in Sec. IV and the variational calculation of the response functions using the method of moments is discussed. The linearized scaling ansatz analysis is given in Sec. V, followed by the its extension to higher-order moments and inclusion of self-energy corrections in Sec. VI. Finally, we discuss the experimental outlook of this work in Sec. VII and conclude the paper with further discussions in Sec. VIII. Most of the technical details and tedious calculations are left to the Appendixes.

II. THE FORMALISM

A. The Hamiltonian

The Hamiltonian for trapped dipolar fermions prepared in a single hyperfine state and placed in a strong polarizing dc field (electric for polar molecules, magnetic for atoms with permanent magnetic dipoles) can be written as

$$H_{\rm 3D} = \int d^3\mathbf{r}\,\psi^\dagger(\mathbf{r})\left(-\frac{\nabla^2}{2m} + U^{\rm 3D}_{\rm trap}(\mathbf{r})\right)\psi(\mathbf{r}) + \int d^3\mathbf{r}\,d^3\mathbf{r}'\,\mathcal{V}^{\rm 3D}_{\rm dip}(\mathbf{r}-\mathbf{r}')\,\psi^\dagger(\mathbf{r})\,\psi^\dagger(\mathbf{r}')\,\psi(\mathbf{r}')\,\psi(\mathbf{r}), \tag{1}$$

where

$$U^{\rm 3D}_{\rm trap}(\mathbf{r}) = \tfrac{1}{2}m\omega_z^2 z^2 + \tfrac{1}{2}m\omega_0^2(x^2+y^2) \tag{2}$$

is the axially symmetric trap potential and

$$\mathcal{V}^{\rm 3D}_{\rm dip}(\mathbf{r}) = \frac{D^2}{|\mathbf{r}|^5}(|\mathbf{r}|^2 - 3z^2). \tag{3}$$

Here, D is the dipole moment. We set $\hbar = 1$ throughout this paper unless it appears explicitly. A schematic picture of the system is shown in Fig. 2. We have assumed that the

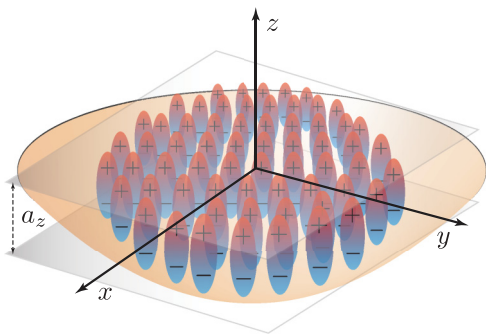

FIG. 2. (Color online) A schematic picture of quasi-2D dipolar fermions in an isotropic in-plane trap. A strong dc field aligns the dipoles along the vertical axis (z). The quasi-2D limit is achieved when $a_z \equiv [\hbar/(m\omega_z)]^{1/2}$ is much smaller than both the interparticle separation $n_{\rm 2D}^{-1/2}$ and the thermal de Broglie wavelength $\lambda_T \equiv h/(2\pi m k_B T)^{1/2}$ (equivalently, when $\omega_z \gg \max\{\epsilon_F, k_B T\}$).

dipoles are fully aligned along the z axis. Here, $\psi^{(\dagger)}(\mathbf{r})$ is the fermion annihilation (creation) operator in 3D space. In the limit $\omega_z \gg \omega_0, \epsilon_F, k_B T$ (where ϵ_F and T denote the Fermi energy and the temperature), the particles occupy only the lowest transverse subband and we can reduce the above 3D Hamiltonian to an effective 2D model:

$$H_{\rm 2D} = \int d^2\mathbf{r}\, \psi_0^\dagger(\mathbf{r}) \left(-\frac{\nabla^2}{2m} + U_{\rm trap}^{\rm 2D}(\mathbf{r}) \right) \psi_0(\mathbf{r}) + \int d^2\mathbf{r}\, d^2\mathbf{r}'\, \mathcal{V}_{\rm dip}^{\rm 2D}(\mathbf{r}-\mathbf{r}')\, \psi_0^\dagger(\mathbf{r})\, \psi_0^\dagger(\mathbf{r}')\, \psi_0(\mathbf{r}')\, \psi_0(\mathbf{r}). \tag{4}$$

Here, $\mathbf{r} = (x, y)$ denote the in-plane 2D coordinates and $\psi_0^{(\dagger)}(\mathbf{r})$ denotes the fermion annihilation (creation) in the lowest subband. We have neglected the constant zero-point energy $\hbar\omega_z/2$. $U_{\rm trap}^{\rm 2D}(\mathbf{r}) = m\omega_0^2(x^2+y^2)/2$ is the in-plane part of the original trap potential and $\mathcal{V}_{\rm dip}^{\rm 2D}(\mathbf{r})$ is the effective dipole-dipole interaction in the lowest subband:

$$\mathcal{V}_{\rm dip}^{\rm 2D}(\mathbf{r}) = \int dz\, dz'\, |\phi_0(z)|^2\, |\phi_0(z')|^2\, \mathcal{V}_{\rm dip}^{\rm 3D}(\mathbf{r}, z-z'), \tag{5}$$

where $\phi_0(z) = e^{-z^2/(2a_z^2)}/(\sqrt{\pi}\, a_z)^{\frac{1}{2}}$ is the transverse wave function of particles in the lowest subband and $a_z \equiv (m\omega_z)^{-1/2}$ is the transverse oscillator length. The above integral can be calculated analytically and we find

$$\mathcal{V}_{\rm dip}^{\rm 2D}(r) = \frac{1}{\sqrt{2\pi}} \frac{D^2}{2a_z^3}\, e^{r^2/(4a_z^2)} \times \left[\left(2 + \frac{r^2}{a_z^2}\right) K_0\left(\frac{r^2}{4a_z^2}\right) - \frac{r^2}{a_z^2} K_1\left(\frac{r^2}{4a_z^2}\right) \right], \tag{6}$$

where $\{K_n(x)\}$ denote the modified Bessel functions of the second kind. In the momentum space, we get

$$\tilde{\mathcal{V}}_{\rm dip}^{\rm 2D}(q) = \frac{2\pi D^2}{a_z} \left[\sqrt{\frac{2}{\pi}} - q a_z e^{q^2 a_z^2/2} \mathrm{Erfc}\left(\frac{q a_z}{\sqrt{2}}\right) \right]. \tag{7}$$

The effective interaction is purely repulsive regardless of the choice for a_z; however, its strength decreases as a_z is increased. We denote $\mathcal{V}_{\rm dip}^{\rm 2D} \equiv \mathcal{V}$, $\tilde{\mathcal{V}}_{\rm dip}^{\rm 2D} \equiv \tilde{\mathcal{V}}$, and $U_{\rm dip}^{\rm 2D} \equiv U$ in the remainder of this paper for brevity.

It is worthwhile to study the behavior of the effective 2D interaction in various limits. For $q a_z \ll 1$, we find:

$$\tilde{\mathcal{V}}(q) \simeq \frac{4\sqrt{2\pi} D^2}{3a_z} - 2\pi D^2 q + O(q^2), \tag{8}$$

whereas for $q a_z \gg 1$, we get

$$\tilde{\mathcal{V}}(q) \simeq -\frac{2D^2\sqrt{2\pi}}{3a_z} \left(1 - \frac{3}{q^2 a_z^2} + O\left(q^{-4} a_z^{-4}\right) \right). \tag{9}$$

Apart from the constant term in Eq. (8), which only contributes to interactions in the s-wave channel and is immaterial here, we find a linear dependence on q. This linear behavior eventually reaches a plateau once $q \sim 1/a_z$. We shall see later that this linear dependence has interesting consequences on the temperature dependence of low-lying collective excitations.

In real space, for small r/a_z, we find a behavior similar to the 2D Coulomb gas:

$$\mathcal{V}(r) \approx \frac{D^2}{\sqrt{2\pi} a_z^3} \left\{ -2 - \gamma - \ln\left[r^2 \big/ \left(8a_z^2\right) \right] + O(r^2 \ln r) \right\}, \tag{10}$$

where γ is the Euler's constant. For large r/a_z, the r^{-3} dipole-dipole interaction is recovered:

$$\mathcal{V}(r) \approx D^2/r^3 + O\left(a_z^2/r^5\right). \tag{11}$$

It is useful to define a "dipolar length":

$$a_d \equiv \frac{m D^2}{\hbar^2}, \tag{12}$$

which is a quantum length scale associated to dipolar interactions. We also define the following useful dimensionless parameters:

$$\lambda_d \equiv \frac{m D^2}{\hbar^2} \left(\frac{m\omega_0}{\hbar} \right)^{\frac{1}{2}}, \quad (2N)^{\frac{1}{4}} \equiv \left(\frac{a_d}{a_0} \right) (2N)^{\frac{1}{4}}, \quad \eta \equiv (2N)^{\frac{1}{4}} \left(\frac{\omega_0}{\omega_z} \right)^{\frac{1}{2}}, \tag{13}$$

where $a_0 \equiv [\hbar/(m\omega_0)]^{\frac{1}{2}}$ is the in-plane oscillator length and N is the number of trapped particles. λ_d is a measure of dipolar interaction strength and is of the order of the typical value of interaction energy over the kinetic energy in the quantum degenerate regime. η is a measure of "quasi-two-dimensionality" and is of the order of the transverse oscillator length a_z divided by the inter-particle separation. The strict 2D limit $\omega_z \to \infty$ corresponds to $\eta = 0$.

B. Linear response theory

A typical experiment for measuring the collective excitations of trapped particles is the following: The gas is prepared in the thermal equilibrium at $t < 0^-$. For $t > 0^-$, the system is subjected to a perturbation such as a kick or modulation of the trap potential and a certain observable is monitored. If the frequency and amplitude of the perturbing potential is small compared to the macroscopic scales, such an experiment can be theoretically investigated within the linear response theory. Let us denote the perturbing potential and the observable as $\delta U(\mathbf{r}, t)$ and $O(\mathbf{r})$, respectively, and their corresponding second quantized operators are $\delta\hat{U} \equiv \int d^2\mathbf{r}\, \psi_0^\dagger(\mathbf{r})\, \delta U(\mathbf{r}, t)\, \psi_0(\mathbf{r})$ and $\hat{O} \equiv \int d^2\mathbf{r}\, \psi_0^\dagger(\mathbf{r})\, O(\mathbf{r})\, \psi_0(\mathbf{r})$. The usual linear response theory then yields

$$\langle \hat{O} \rangle_t = \int_{0^-}^{t} dt' \int d^2\mathbf{r}\, d^2\mathbf{r}'\, \chi_{\rm dd}^R(\mathbf{r}, \mathbf{r}'; t-t')\, O(\mathbf{r})\, \delta U(\mathbf{r}', t'), \tag{14}$$

where $\chi_{\rm dd}^R(\mathbf{r}, \mathbf{r}'; t-t')$ is the retarded density-density response function:

$$\chi_{\rm dd}^R(\mathbf{r}, \mathbf{r}'; t-t') \equiv -i\theta(t-t') \mathrm{Tr}\{\hat{\rho}_0[\hat{\rho}(\mathbf{r}, t), \hat{\rho}(\mathbf{r}', t)]\}, \tag{15}$$

where $\hat{\rho}(\mathbf{r}, t) = \psi_0^\dagger(\mathbf{r}, t)\psi_0(\mathbf{r}, t)$ is the density operator and $\hat{\rho}_0$ is the initial density matrix. At this stage, one may choose a proper many-body approximation scheme and attempt to

evaluate the response function using the diagram technique. However, the lack of translational symmetry due to the presence of the trap potential makes this approach complicated. In practice, one will have to make assumptions about separation of microscopic and macroscopic time and length scales in order to make the calculations tractable. It is, however, much more transparent to acknowledge the existence of such a separation of scales from the outset and reduce the complicated evolution equations of the nonequilibrium Green's functions to quantum kinetic equations. One may then evaluate the linear response functions directly using the quantum kinetic equations. We describe this method in the next section, where we also briefly review the quantum kinetic equations approach.

We conclude this section by defining the response functions relevant to monopole and quadrupole oscillation experiments. The monopole oscillations can be excited by choosing $\delta U(\mathbf{r},t) \equiv \delta U_m(\mathbf{r},t) \equiv \mathcal{A}(t)\, m\omega_0^2 r^2$, where $\mathcal{A}(t)$ is the temporal shape of the perturbation (e.g., a δ function, a finite pulse or a periodic modulation). We choose $\mathcal{A}(t) \equiv \mathcal{A}_0\, \omega_0^{-1} \delta(t)$ for concreteness. The linear response to any other pulse shape can be determined from the impulse response. Note that we have "defined" the monopole oscillations as the response of the trapped gas to $\sim r^2$ perturbation. One may choose any other isotropic trap perturbation (such as r^4, etc.). Such choices, however, excite higher-order modes to a greater degree, which may not be desirable. Here, the observable is the variation in the size of the cloud, $\hat{r}^2 - \langle \hat{r}^2 \rangle_0$. We define the "monopole response function" as

$$\chi_{r^2}(t) = \mathcal{A}_0^{-1} m\omega_0\, \theta(t)(\langle \hat{r}^2 \rangle_t - \langle \hat{r}^2 \rangle_0). \tag{16}$$

Likewise, we define the quadrupole oscillations as the response of the trapped gas to $\delta U(\mathbf{r},t) \equiv \delta U_q(\mathbf{r},t) \equiv \mathcal{A}(t)\, m\omega_0^2 (x^2 - y^2)$ and define the "quadrupole response function" as

$$\chi_{x^2-y^2}(t) = \mathcal{A}_0^{-1} m\omega_0\, \theta(t)\, \langle \hat{x}^2 - \hat{y}^2 \rangle_t. \tag{17}$$

Note that $\langle \hat{x}^2 - \hat{y}^2 \rangle_0 = 0$ due to the isotropy of the trap.

C. From quantum kinetic equations to the collsional Boltzmann-Vlasov equation

Quite generally, the dynamics of confined quantum gases can be formulated and studied using the formalism of nonequilibrium Green's functions, that is, either by solving Kadanoff-Baym equations within a relevant conserving approximation [19] or by using the Keldysh-Schwinger diagram technique. Such formulations in their fullest generality, however, are only necessary when the spatial and temporal scales of inhomogeneities (the trap and its perturbation) is comparable to the microscopic scales. In experiments dealing with a large number of particles N in shallow traps, there is a natural separation of temporal and spatial scales between the microscopic (single particle) and macroscopic (collective) dynamics. Exploiting this fact, one can reduce the complicated Kadanoff-Baym equations to the intuitive picture of quantum kinetic equations using the well-known procedure of gradient expansion [19,36]. There exist several decent treatments of this subject in the literature and we refer the reader to the excellent pioneering monograph by Kadanoff and Baym [19] and Ref. [36] for details. For the purpose self-containedness and in order to clarify the nature of approximations, however, we provide a brief overview of the basic elements of the kinetic theory. Our starting point is the general quantum kinetic equation for a system composed of a single species of fermions (i.e., a gas prepared in a single hyperfine state):

$$[\mathrm{Re}(G^{-1})^+, iG^{\gtrless}] - [i\Sigma^{\gtrless}, \mathrm{Re}G^+] = G^< \Sigma^> - G^> \Sigma^<, \tag{18}$$

where $G^+(\mathbf{p},\omega;\mathbf{r},t) \equiv (\omega - p^2/(2m) - U(\mathbf{r},t) - \Sigma^+)^{-1}$ and $G^{\gtrless}(\mathbf{p},\omega;\mathbf{r},t)$ are the retarded and greater or lesser nonequilibrium Green's functions in the mixed Wigner coordinates [36]. Here, $U(\mathbf{r},t)$ is the external potential (i.e., the trap potential and its perturbation) and is assumed to vary on a scale much larger than the microscopic scales. $\Sigma^+(\mathbf{p},\omega;\mathbf{r},t)$ and $\Sigma^{\gtrless}(\mathbf{p},\omega;\mathbf{r},t)$ are the retarded and greater/lesser self-energies. In the mixed Wigner coordinates, $(\mathbf{p},\omega)$ and $(\mathbf{r},t)$ denote to the Fourier transformed fast microscopic coordinates and the slow macroscopic coordinates, respectively. $[A,B]$ is the generalized Poisson's bracket:

$$[A,B] = \partial_\omega A\, \partial_t B - \partial_t A\, \partial_\omega B - \nabla_{\mathbf{p}} A \cdot \nabla_{\mathbf{r}} B + \nabla_{\mathbf{r}} A \cdot \nabla_{\mathbf{p}} B. \tag{19}$$

It is generally understood that G^+ encodes the spectral properties of the system (single-particle states) while $G^<$ and $G^>$ contains the information about the statistics of particles and holes, respectively. Likewise, the real and imaginary parts of Σ^+ describe the renormalization of the single-particle dispersion and the spectral broadening, respectively, while $\Sigma^<$ and $\Sigma^>$ describe the scattering-in and -out rates. In analogy to the equilibrium case, it is fruitful to introduce the local spectral function $A(\mathbf{p},\omega;\mathbf{r},t)$, Wigner's function $f(\mathbf{p},\omega;\mathbf{r},t)$, and spectral broadening $\Gamma(\mathbf{p},\omega;\mathbf{r},t)$ (hereafter, we drop the common arguments of the functions unless it is necessary), such that $G^< \equiv iAf$, $A \equiv i(G^> - G^<) \equiv -2\,\mathrm{Im}(G^+)$ and $\Gamma \equiv i(\Sigma^> - \Sigma^<) \equiv -2\,\mathrm{Im}(\Sigma^+)$. The kinetic equations can be partially integrated to yield $(G^+)^{-1} = \omega - p^2/(2m) - \mathrm{Re}(\Sigma^+) + i\Gamma/2$. This partial integration, along with one's choice of a many-body approximation that gives the self-energies as a functional of $G^<$ and $G^>$ and finally the kinetic equation [Eq. (18)] constitute a closed set of partial integro-differential equations for f and A whose solution describes the slow nonequilibrium dynamics of the system. For the case of self-consistent many-body approximations, the kinetic equation obeys differential conservation laws for mass, momentum, and energy currents. The existence and satisfaction of such conservation laws are necessary for formation and propagation of collective modes [19].

Although the formalism of quantum kinetic equations is much simpler than a full nonequilibrium treatment, it is still extremely difficult to solve such equations in practice without resorting to further approximations. One useful approximation relevant for weakly interacting systems is the quasiparticle approximation. The idea is that in the quantum degenerate regime, only the particle-hole excitations near the Fermi surface are responsible for the slow dynamics. The lifetime of such excitations, $\Gamma^{-1}(p_F,\epsilon_F)$, is proportional to T_F^2/T^2, which can be very large. Thus, one may neglect the spectral broadening of the Green's functions appearing in the Poisson brackets as a reasonable approximation, and approximate the spectral function as $A \approx 2\pi\delta[\omega - p^2/(2m) - U - \Sigma^+]$. This

approximation yields an ansatz for the greater/lesser Green's functions:

$$G^{<}_{\rm qp}(\mathbf{p},\omega;\mathbf{r},T) = 2\pi i\, Z_{\mathbf{p}}\, \delta(\omega - E_{\mathbf{p}})\, n(\mathbf{p};\mathbf{r},t),$$
$$G^{>}_{\rm qp}(\mathbf{p},\omega;\mathbf{r},T) = -2\pi i\, Z_{\mathbf{p}}\, \delta(\omega - E_{\mathbf{p}})\, [1 - n(\mathbf{p};\mathbf{r},t)], \tag{20}$$

where $E_{\mathbf{p}}$ is the (local) quasiparticle dispersion and is implicitly given by $\omega - p^2/(2m) - U(\mathbf{r},t) - \Sigma^{+}(\mathbf{p},E_{\mathbf{p}};\mathbf{r},t) = 0$ and $Z_{\mathbf{p}} = [1 - \partial_\omega \Sigma^{+}(\mathbf{p},\omega = E_{\mathbf{p}};\mathbf{r},t)]^{-1}$ is the (local) quasiparticle residue. $n(\mathbf{p};\mathbf{r},t) \equiv f(\mathbf{p},E_{\mathbf{p}};\mathbf{r},t)$ is the quasiparticle occupation number. Plugging this ansatz into the kinetic equation, we obtain the collisional Boltzman-Vlasov (CBV) equation:

$$\Big(\frac{\partial}{\partial t} + \frac{\mathbf{p}}{m}\cdot\boldsymbol{\nabla}_{\mathbf{r}} + \boldsymbol{\nabla}_{\mathbf{p}}\Sigma^{+}[n]\cdot\boldsymbol{\nabla}_{\mathbf{r}} - \boldsymbol{\nabla}_{\mathbf{r}}\Sigma^{+}[n]\cdot\boldsymbol{\nabla}_{\mathbf{p}} - \boldsymbol{\nabla}_{\mathbf{r}}U(\mathbf{r},t)\cdot\boldsymbol{\nabla}_{\mathbf{p}}\Big) n(\mathbf{p};\mathbf{r},t) = I_c[n]. \tag{21}$$

$I_c[n]$ is called the collision integral operator and is given by

$$I_c[n] \equiv -i\, Z_{\mathbf{p}}[(1-n)\,\Sigma^{<} + n\,\Sigma^{>}]. \tag{22}$$

The CBV equation can be thought of as a generalization of the usual Boltzmann transport equation of classical gases by (1) including Pauli exclusion in the collision integral and (2) using dressed quasiparticle. A crucial observation made by Kadanoff and Baym is that the one may use different conserving many-body approximations for left-hand (known as convective or dynamical) and the right-hand (collisional) sides of the kinetic equation without breaking the conservation laws. Intuitively, the dynamical and collisional contributions describe different physics, and as long as each respect the conservation laws, the conserving property of the kinetic equation is preserved as a whole.

The main goal of this work is to study the effect of dipolar interactions to the leading order in the interaction strength on both CL quasiparticle transport and elastic quasiparticle collisions. We use the self-consistent Hartree-Fock (HF) approximation on the dynamical side and the Born approximation to describe collisions. The retarded self-energy in the HF approximation is instantaneous and is given by

$$\Sigma^{+}[n](\mathbf{p};\mathbf{r},t) = \int d^2\mathbf{r}'\, \frac{d^2\mathbf{p}'}{(2\pi)^2}[\mathcal{V}(\mathbf{r}-\mathbf{r}') - \delta^2(\mathbf{r}-\mathbf{r}')\tilde{\mathcal{V}}(\mathbf{p}-\mathbf{p}')] n(\mathbf{p}';\mathbf{r}',t), \tag{23}$$

where $\mathcal{V}(\mathbf{r})$ and $\tilde{\mathcal{V}}(\mathbf{p})$ are the two-body interactions in the real and momentum space. Dealing with long-range interactions, we have included nonlocal contributions in the Hartree term. Such contributions are beyond the first-order gradient approximation but their inclusion may be necessary for long-range interactions. It is exactly the inclusion of such nonlocal contributions in the Boltzmann-Vlasov equation for electron liquids that yields plasmon modes and Landau damping. However, we will shortly show that nonlocal direct interactions are negligible in the case of dipole-dipole interactions. Also, note that since Σ^{+} has no ω dependence, the quasiparticle residue is 1. The collision integral in the Born approximation is given by [36]

$$I_c[n] = \int \frac{d^2\mathbf{p}_1}{(2\pi)^2}\frac{d^2\mathbf{p}'}{(2\pi)^2}\frac{d^2\mathbf{p}'_1}{(2\pi)^2}(2\pi)^2\delta^2(\Delta\mathbf{P})(2\pi)\delta(\Delta E) \times \frac{1}{2}|\mathcal{M}|^2[(1-n)(1-n_1)n'n'_1 - nn_1(1-n') \times (1-n'_1)], \tag{24}$$

where $\mathcal{M} = \tilde{\mathcal{V}}(\mathbf{p}-\mathbf{p}') - \tilde{\mathcal{V}}(\mathbf{p}-\mathbf{p}'_1)$ is the Born scattering amplitude, $\Delta\mathbf{P} = \mathbf{p} + \mathbf{p}_1 - \mathbf{p}' - \mathbf{p}'_1$ and $\Delta E = E_{\mathbf{p}} + E_{\mathbf{p}_1} - E_{\mathbf{p}'} - E_{\mathbf{p}'_1}$. Note that $E_{\mathbf{p}} = p^2/(2m) + U(\mathbf{r},t) + \Sigma^{+}[n](\mathbf{p};\mathbf{r},t)$. We have also used the shorthand $n \equiv n(\mathbf{p};\mathbf{r},t)$, $n_1 \equiv n(\mathbf{p}_1;\mathbf{r},t)$, etc., in the above equation.

We conclude this section by discussing the validity of the approximations adopted so far. Since we have described the interactions using the lowest-order processes, the predictions are quantitatively reliable only as long as the system is in the weakly interacting regime, that is, $\lambda_d \ll 1$ [see Eq. (13)]. For dipolar interactions, this condition is equivalent to diluteness $\sqrt{\rho}a_d \ll 1$, where ρ is the 2D density and a_d is the dipolar length defined earlier [Eq. (12)]. Since the Fermi liquid state is expected to be stable for a wide range of interaction strengths (up to the crystallization point), we do not expect the higher-order many-body corrections to lead to qualitatively different physics. Therefore, although our approximations are only controlled in the dilute limit, we allow ourselves to extend our analysis to $\lambda_d \sim O(1)$ as well.

Apart from the many-body physics, the validity of Born approximation in describing two-body scatterings and the negligence of multiple scatterings must also be assessed. The Born approximation is valid when $\hbar v \gg \mathcal{V}a$, where v is the typical velocity of the scattering pairs in the center of mass frame and a is range of interactions. Identifying a with a_d and $v \sim [m\max(k_BT, k_BT_F)]^{\frac{1}{2}}$, this condition implies

$$\max(k_BT, k_BT_F) \ll k_BT_{\rm dip} \equiv \frac{\hbar^2}{ma_d^2}, \tag{25}$$

where we have defined a "dipolar temperature" $T_{\rm dip}$. This is precisely the condition for near-threshold scatterings. The dipolar scatterings in 2D is studied in detail in Ref. [28] and it is shown that the Born approximation is quantitatively reliable provided that $mva_d/\hbar \lesssim 0.1$. Inclusion of multiple scatterings, however, results in significant quantitative corrections as one approaches the semiclassical regime and the Born approximation consistently found to overestimate the cross section. In this paper, we confine our analysis to near-threshold scatterings. Therefore, the quantitative validity of our results crucially relies on Eq. (25). Here, we assume that the following scale separation holds:

$$T_F \ll T_{\rm dip} \quad \Leftrightarrow \quad \frac{a_0}{a_d} \gg N^{\frac{1}{4}}, \tag{26}$$

so that we can allow ourselves to investigate both the quantum degenerate regime ($T/T_F \ll 1$) and the thermal regime ($T/T_F \gg 1$) up to $T \sim T_{\rm dip}$. We note that this condition is satisfied well in the current experiments with both polar molecules and rare-earth atoms (see Sec. VII).

III. THE EQUILIBRIUM STATE

The first step in the linear response analysis using the kinetic equations is to determine the equilibrium distribution about which the perturbation analysis is carried out. We assume that the system has reached a thermal equilibrium state in the external potential $U(\mathbf{r}) = m\omega_0^2 r^2/2$ before the perturbation is introduced. It is easily shown that the CBV equation has a unique equilibrium solution given by

$$n_0(p;r) = \left\{\exp\left[\beta\left(\frac{p^2}{2m} + \Sigma_0(p;r) + \frac{1}{2}m\omega_0^2 r^2 - \mu\right)\right] + 1\right\}^{-1}, \tag{27}$$

where we have introduced the shorthand $\Sigma_0 \equiv \Sigma^+[n_0]$. The above equation has to be solved self-consistently along with the expression for the self-energy [Eq. (23)]. It is easily verified that the above solution satisfies $I_c[n_0] = 0$ and at the same time, it solves the left-hand side of the CBV equation. The global chemical potential μ has to be found such that the equilibrium distribution function yields the correct number of trapped particles:

$$\int d\Gamma\, n_0(\mathbf{p};\mathbf{r}) = N, \tag{28}$$

where we have defined the phase-space volume differential as $d\Gamma \equiv d^2\mathbf{r}\, d^2\mathbf{p}/(2\pi)^2$. In the case of harmonic traps, it is useful to define the following scaled coordinates:

$$\bar{\mathbf{r}} \equiv \frac{\mathbf{r}}{r_0}, \quad r_0 \equiv [2N/(m\omega_0)^2]^{1/4}, \qquad \bar{\mathbf{p}} \equiv \frac{\mathbf{p}}{p_0}, \quad p_0 \equiv [2N(m\omega_0)^2]^{1/4}. \tag{29}$$

In the scaled coordinates, the equation for the particle number is $\int d\bar{\Gamma}\, n_0(\bar{\mathbf{p}};\bar{\mathbf{r}}) = 1/2$, where $d\bar{\Gamma} \equiv d^2\bar{\mathbf{r}}\, d^2\bar{\mathbf{p}}/(2\pi)^2 = d\Gamma/(2N)$. The equilibrium distribution function also reads as

$$n_0(\bar{\mathbf{p}};\bar{\mathbf{r}}) = \left\{\exp\left[\bar{\beta}\left(\frac{\bar{p}^2 + \bar{r}^2}{2} + \bar{\Sigma}_0(\bar{r};\bar{p}) - \bar{\mu}\right)\right] + 1\right\}^{-1}, \tag{30}$$

where $\bar{\beta} = T_F/T$ and

$$T_F = (2N)^{\frac{1}{2}}\frac{\hbar\omega_0}{k_B} \tag{31}$$

is the (in-trap) Fermi temperature, $\bar{\mu} = \mu/(k_B T_F)$ is the dimensionless chemical potential, and

$$\bar{\Sigma}^+[n](\bar{\mathbf{p}};\bar{\mathbf{r}},t) = \omega_0^{-1}\int d\bar{\Gamma}'[\sqrt{2N}\,\mathcal{V}[r_0(\bar{\mathbf{r}} - \bar{\mathbf{r}}')] - m\omega_0\delta^2(\bar{\mathbf{r}} - \bar{\mathbf{r}}')\tilde{\mathcal{V}}[p_0(\bar{\mathbf{p}} - \bar{\mathbf{p}}')]]n(\bar{\mathbf{p}}';\bar{\mathbf{r}}',t) \tag{32}$$

is the dimensionless self-energy functional. Also, $\bar{\Sigma}_0 \equiv \bar{\Sigma}^+[n_0]$. The motivation for using scaled coordinates becomes clear upon investigating the equilibrium state of the noninteracting problem. In this case, the (dimensionless) equilibrium density $\bar{\rho}_0^{(0)}(\bar{r})$ can be found analytically,

$$\bar{\rho}_0^{(0)}(\bar{r}) \equiv \int \frac{d^2\bar{\mathbf{p}}}{(2\pi)^2}\,\bar{n}_0(\bar{p};\bar{r}) = \ln\left[1 + e^{\bar{\beta}(\bar{\mu} - \bar{r}^2/2)}\right]/(2\pi\bar{\beta}), \tag{33}$$

using which we obtain an equation for the chemical potential of the noninteracting trapped gas:

$$\bar{\mu}^2 + \frac{\pi^2}{3}\bar{T}^2 + 2\,\bar{T}^2\,\mathrm{Li}_2[-\exp(-\bar{\mu}/\bar{T})] = 1, \tag{34}$$

where $\bar{T} = T/T_F$. At low temperatures, the above equation admits the solution $\bar{\mu} = 1 - \pi^2\bar{T}^2/6 + O(\bar{\beta}^{-2}e^{-\bar{\beta}})$. The zero-temperature Thomas-Fermi radius of the cloud is easily obtained from Eq. (33), yielding $R_{\mathrm{TF}}^{(0)} = [2\sqrt{2N}/(m\omega_0)]^{1/2} \equiv \sqrt{2}\,r_0$. Also, the Fermi momentum at the center of the trap is given by $p_F^{(0)} = [2\sqrt{2N}(m\omega_0)]^{1/2} \equiv \sqrt{2}\,p_0$. We note that N does not appear explicitly in the expressions written in terms of the scaled coordinates. Moreover, at low temperatures, the equilibrium distribution function is only appreciably larger than zero in a region of size $O(1)$ in the scaled phase-space coordinates.

Once the interactions are taken into account, analytical solutions can no longer be obtained and the equilibrium distribution function has to found numerically. It is, however, useful to investigate the effect of nonlocal Hartree self-energy term first: The forthcoming calculations will be significantly simplified if the nonlocal effects can be neglected. Carrying out the trivial momentum integration in the first term of Eq. (32), the Hartree self-energy can be expressed as a linear functional of just the density:

$$\bar{\Sigma}_H^+[\bar{\rho}](\bar{\mathbf{r}},t) = \omega_0^{-1}\int d^2\bar{\mathbf{r}}'\,\sqrt{2N}\,\mathcal{V}(r_0\bar{\mathbf{r}}')\,\bar{\rho}(\bar{\mathbf{r}} - \bar{\mathbf{r}}',t). \tag{35}$$

Observing that the density is only appreciable in a region of size $O(1)$ in the scaled coordinates and the appearance of $r_0 \sim N^{1/4}$ in the argument of interaction potential, the above integral is expected to only depend of the values of the density within a small region of size $\sim N^{-1/4}$ about $\bar{\mathbf{r}}$. Assuming that the density variation is smooth, we may expand $\bar{\rho}$ to quadratic order about $\bar{\mathbf{r}}$ to get

$$\bar{\Sigma}_H^+[\bar{\rho}](\bar{\mathbf{r}},t) \approx \omega_0^{-1}\int d^2\bar{\mathbf{r}}'\,\sqrt{2N}\,\mathcal{V}(r_0\bar{\mathbf{r}}') \times[\bar{\rho}(\bar{\mathbf{r}},t) - \bar{\mathbf{r}}'\cdot\nabla\bar{\rho}(\bar{\mathbf{r}},t) + \bar{r}'_\alpha\bar{r}'_\beta\partial_\alpha\partial_\beta\bar{\rho}(\bar{\mathbf{r}},t)/2]. \tag{36}$$

The first contribution is the usual local density approximation (LDA):

$$\bar{\Sigma}_{H,\mathrm{LDA}}^+[\bar{\rho}](\bar{\mathbf{r}},t) \equiv \sqrt{2N}\omega_0^{-1}\bar{\rho}(\bar{\mathbf{r}},t)\int d^2\bar{\mathbf{r}}'\;\mathcal{V}(r_0\bar{\mathbf{r}}') = m\,\tilde{\mathcal{V}}(0)\,\bar{\rho}(\bar{\mathbf{r}},t). \tag{37}$$

The gradient term vanishes due to the isotropy of $\mathcal{V}(\mathbf{r})$. The quadratic term is dominated by the long-range behavior of $\mathcal{V}(\mathbf{r})$ assuming that the short-range part of $\mathcal{V}(\mathbf{r})$ is integrable [which is the case for dipolar interactions; see Eq. (10)]. Observing that the Hessian matrix of the density is also $O(1)$ in the scaled coordinates, we easily find that the quadratic term yields a correction that scales like $N^{1/2-\alpha/4}$ for a potential with

power-law tail $\mathcal{V}(\mathbf{r}) \sim r^{-\alpha}$. For dipolar interactions, $\alpha = 3$ and we find that the leading corrections to LDA scale like $N^{-1/4}$ and can be neglected for large N. Note that if we were dealing with an electron gas ($\alpha = 1$), such corrections would grow larger with N and the nonlocal Hartree functional had to be kept untouched. A direct result of this simple analysis is that the Landau damping, which is driven by nonlocal direct interactions, is expected to be absent in a dipolar Fermi gas in the thermodynamic limit. In the remainder of this paper, we treat the Hartree potential in the LDA approximation and use the following local self-energy functional:

$$\begin{aligned}\bar{\Sigma}^{+}_{\mathrm{LDA}}[n](\bar{\mathbf{p}};\bar{\mathbf{r}},t) &= m\int \frac{d^2\bar{\mathbf{p}}'}{(2\pi)^2}[\tilde{\mathcal{V}}(0)-\tilde{\mathcal{V}}[p_0(\bar{\mathbf{p}}-\bar{\mathbf{p}}')]]n(\bar{\mathbf{p}}';\bar{\mathbf{r}}',t)\\ &= \lambda_d\int \frac{d^2\bar{\mathbf{p}}'}{(2\pi)^2}\,u(|\bar{\mathbf{p}}-\bar{\mathbf{p}}'|,\eta)\,n(\bar{\mathbf{p}}';\bar{\mathbf{r}}',t),\end{aligned} \tag{38}$$

where we have used Eq. (7) in the second line and have defined:

$$u(x,\eta) = 2\pi x\,\mathrm{Erfcx}\left(\frac{x\eta}{\sqrt{2}}\right), \tag{39}$$

where $\mathrm{Erfcx}(x) \equiv e^{x^2}\mathrm{Erfc}(x)$. The dimensionless parameters λ_d and η were defined earlier [Eq. (13)]. Note that the dependence on N enters the equations only through these two dimensionless parameters.

We obtain the equilibrium distribution function using a simple iterative method. At the initial step, we set $\bar{\Sigma}_0 = 0$ and define the function $n_0(\bar{\mu}) \equiv n[\bar{\Sigma}_0,\bar{\mu}]$, that is, the distribution function obtained using the self-energy $\bar{\Sigma}_0 = 0$ and chemical potential $\bar{\mu}$. We find μ_0 such that $\int d\bar{\Gamma}\, n_0(\mu_0) = 1/2$. To proceed from the ith step to the $(i+1)$th step, we set $\bar{\Sigma}_{i+1} = \bar{\Sigma}^{+}[n_i]$, define $n_{i+1}(\bar{\mu}) \equiv n[\bar{\Sigma}_{i+1},\bar{\mu}]$, and find $\bar{\mu}_{i+1}$ such that $\int d\Gamma'\, n_{i+1}(\bar{\mu}_{i+1}) = 1/2$. At the end of this step, we set $n_{i+1} \to (1-\delta)n_i + \delta\, n_{i+1}$, where $0 < \delta < 1$. The last step is to stabilize the iterative procedure and to damp possible oscillations that prevent convergence. With an arbitrary choice $\delta = 0.75$, we found the this iterative procedure converges to a fixed point in less than ten steps within a relative error tolerance of 10^{-8}. It is trivial to show that the fixed point is indeed the solution.

Figure 3 shows the equilibrium quasiparticle distribution function as a function of $\bar{p}$ and $\bar{r}$ for several values of $\bar{T}$ and λ_d. As one expects, the presence of interactions results in the expansion of the gas in the trap [compare panels (a) and (b)] and thermal fluctuations smear the Fermi surface [compare panels (a) and (c)].

The equilibrium density is shown in Fig. 4(a). The nearly Gaussian distribution around the edge of the trap at finite temperatures and the reduction of the density at the center of the trap at low temperatures due to repulsive interactions can be clearly seen. We also compare the LDA and full nonlocal Hartree self-energy functionals in Fig. 4(b) for various number of particles in the trap. The relative correction to the LDA predictions is of the order of 10^{-3} for a realistic number of trapped particles and, as argued earlier, becomes smaller for larger system sizes.

Having found the equilibrium state, we can move on to the investigation of the low lying collective excitations. To this end, we discuss the linear response theory of the CBV equation in the next section as a first step.

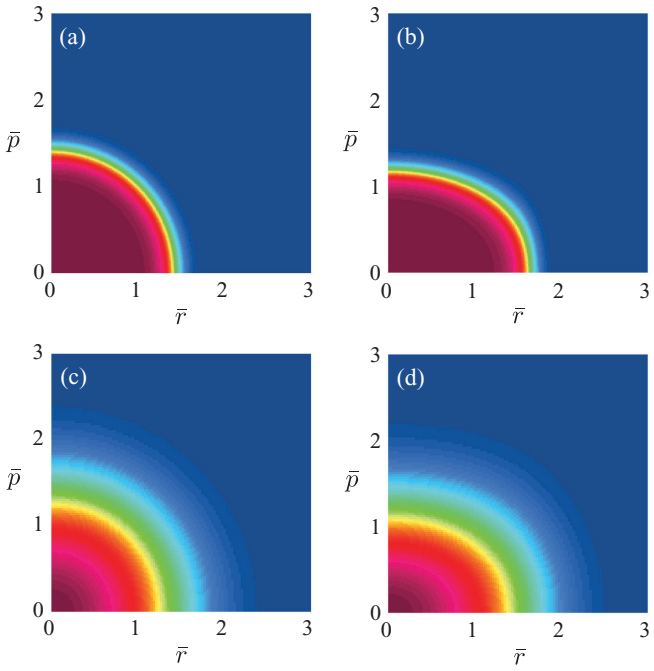

FIG. 3. (Color online) Equilibrium quasiparticle distribution function of quasi-2D dipolar fermions for different temperatures and interactions strengths ($\omega_z = 2\pi \times 23\,\mathrm{kHz}$, $\omega_0 = 2\pi \times 36\,\mathrm{Hz}$, $N = 2200$ in all cases). (a) $T/T_F = 0.1$, $\lambda_d = 0$; (b) $T/T_F = 0.1$, $\lambda_d = 1$; (c) $T/T_F = 0.5$, $\lambda_d = 0$; (d) $T/T_F = 0.5$, $\lambda_d = 1$. Red and blue regions (near to and far from the origin, respectively) correspond to occupied and empty states.

IV. ANALYSIS OF THE COLLECTIVE MODES: LINEAR RESPONSE THEORY OF THE COLLISIONAL BOLTZMANN-VLASOV EQUATION

The linear response can be conveniently evaluated using kinetic equations by introducing a perturbation to the external potential, linearizing the resulting equation about deviations from the global equilibrium state, $\delta n(\bar{\mathbf{p}};\bar{\mathbf{r}},t) \equiv n(\bar{\mathbf{p}};\bar{\mathbf{r}},t) - n_0(\bar{p};\bar{r})$, and solving the resulting linear integro-differential equation. The benefit of this formulation compared to the diagram technique is the possibility of obtaining approximate solutions using well-known variational methods.

Since we are mostly concerned with low temperatures here, it is beneficial to introduce the following ansatz for δn:

$$\delta n(\bar{\mathbf{p}};\bar{\mathbf{r}},t) \equiv \theta(t)\,\Delta_0(\bar{p};\bar{r})\,\Phi(\bar{\mathbf{p}};\bar{\mathbf{r}},t), \tag{40}$$

where $\Delta_0 \equiv \partial n_0/\partial\bar{\mu} = \bar{\beta} n_0(1-n_0)$. The above ansatz is not restrictive for $T > 0$ since $\Delta_0 > 0$ everywhere on the phase space. The only exception is $T = 0$, where Δ_0 restricts the deviations to the local Fermi surface. This is, in fact, a favorable feature since the low-lying collective modes are formed from the particle-hole excitations about the Fermi surface at $T = 0$. Also, at finite T, Δ_0 is sharply peaked about the local Fermi surface and allows the solution of the linearized CBV equation to be representable with a smooth choice of Φ [20]. As we shall see, this feature allows us to construct decent

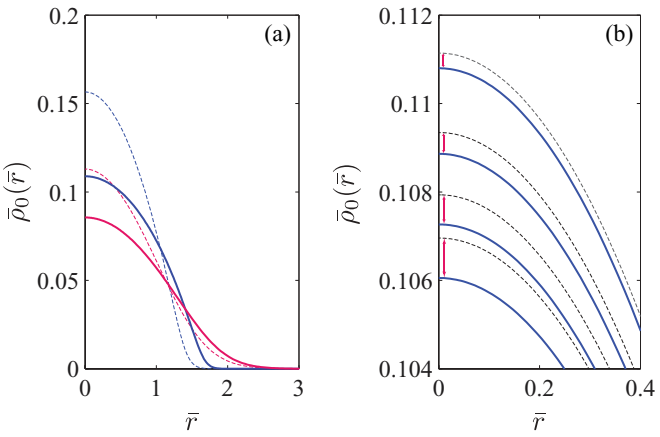

FIG. 4. (Color online) Equilibrium density of a quasi-2D dipolar Fermi gas as a function of the distance from the center of the trap ($\omega_z = 2\pi \times 23\,\mathrm{kHz}$, $\omega_0 = 2\pi \times 36\,\mathrm{Hz}$). (a) Dashed and solid lines correspond to the noninteracting ($\lambda_d = 0$) and interacting ($\lambda_d = 1$), blue (top) and red (bottom) lines correspond to $T/T_F = 0.1$ and 0.5 respectively. In all cases, $N = 2200$. (b) A comparison between the equilibrium densities obtained from LDA (solid lines) and nonlocal (dashed lines) Hartree self-energy functionals. From bottom to top, $N = 500$, 1000, 2200, and 5000. $\lambda_d = 1$ and $T/T_F = 0.1$ in all cases. The nonlocal corrections are clearly negligible and become smaller as N is increased.

approximate solutions by choosing a linear combination of smooth functions as a variational ansatz for Φ.

Plugging this ansatz into the CBV equation, expanding to first order in Φ, and taking a Fourier transform in time, we obtain the following linear integral equation for $\Phi(\bar{\mathbf{p}};\bar{\mathbf{r}},\omega)$:

$$-i\,\bar{\omega}\,\Delta_0\Phi + \mathscr{D}[\Phi] - \mathscr{I}[\Phi] = -(2N)^{-\frac{1}{2}}\{n_0,\delta U(r_0\bar{\mathbf{r}},\omega)\}, \tag{41}$$

where $\{\phi,\psi\} \equiv \nabla_{\bar{\mathbf{r}}}\phi\cdot\nabla_{\bar{\mathbf{p}}}\psi - \nabla_{\bar{\mathbf{p}}}\phi\cdot\nabla_{\bar{\mathbf{r}}}\psi$ is the Poisson bracket with respect to the scaled phase-space coordinates, and $\bar{\omega} \equiv \omega/\omega_0$. $\mathscr{D}[\Phi]$ describes the CL self-consistent mean-field dynamics of quasiparticles:

$$\begin{aligned}\mathscr{D}[\Phi] &= \Delta_0\{\Phi,\bar{\mathcal{H}}_0\} + \{n_0,\bar{\Sigma}[\Delta_0\Phi]\}\\ &= \Delta_0\{\Phi + \bar{\Sigma}[\Delta_0\Phi],\bar{\mathcal{H}}_0\},\end{aligned} \tag{42}$$

where $\bar{\mathcal{H}}_0 = (\bar{p}^2+\bar{r}^2)/2 + \bar{\Sigma}_0$. To get the second line, we have used the identity $\{n_0,\mathcal{A}\} \equiv -\Delta_0\{\bar{\mathcal{H}}_0,\mathcal{A}\}$, which can be easily proved by direct calculation and is valid for arbitrary $\mathcal{A}$.

The first term in the first line of Eq. (42) describes the evolution of quasiparticles in the equilibrium mean field, whereas the second term describes their dynamics in the self-consistently generated residual mean field $\bar{\Sigma}[\Delta_0\Phi]$. $\mathscr{I}[\Phi]$ describes the collisional dynamics and can be written as

$$\begin{aligned}\mathscr{I}[\Phi] = -\frac{\bar{\beta}(2N)^{\frac{1}{2}}}{2}\int \frac{d^2\bar{\mathbf{p}}_1}{(2\pi)^2}\frac{d^2\bar{\mathbf{p}}'}{(2\pi)^2}\frac{d^2\bar{\mathbf{p}}'_1}{(2\pi)^2}(2\pi)^2\delta^2(\Delta\bar{\mathbf{P}})\\ \times(2\pi)\delta(\Delta\bar{E})\,|\bar{\mathcal{M}}|^2\,\mathrm{S}\{\Phi\}\,n_0n_{0,1}(1-n'_0)(1-n'_{0,1}),\end{aligned} \tag{43}$$

where $\Delta\bar{E} \equiv \bar{\mathcal{H}}_0(\bar{\mathbf{p}},\bar{\mathbf{r}}) + \bar{\mathcal{H}}_0(\bar{\mathbf{p}}_1,\bar{\mathbf{r}}) - \bar{\mathcal{H}}_0(\bar{\mathbf{p}}',\bar{\mathbf{r}}) - \bar{\mathcal{H}}_0(\bar{\mathbf{p}}'_1,\bar{\mathbf{r}})$, $\Delta\bar{\mathbf{P}} \equiv \bar{\mathbf{p}} + \bar{\mathbf{p}}_1 - \bar{\mathbf{p}}' - \bar{\mathbf{p}}'_1$, $\bar{\mathcal{M}} = m(\tilde{\mathcal{V}}[p_0(\bar{\mathbf{p}}-\bar{\mathbf{p}}')] - \tilde{\mathcal{V}}[p_0(\bar{\mathbf{p}}-\bar{\mathbf{p}}'_1)])$, and $\mathrm{S}[\Phi] \equiv \Phi(\bar{\mathbf{p}};\bar{\mathbf{r}},\omega) + \Phi(\bar{\mathbf{p}}_1;\bar{\mathbf{r}},\omega) - \Phi(\bar{\mathbf{p}}';\bar{\mathbf{r}},\omega) - \Phi(\bar{\mathbf{p}}'_1;\bar{\mathbf{r}},\omega)$. Note that the dressed quasiparticle dispersions have been used in the collision integrals. Specializing to the case of dipole-dipole interactions, we get

$$|\bar{\mathcal{M}}|^2 = \lambda_d^2[u(|\bar{\mathbf{p}}-\bar{\mathbf{p}}'|,\eta) - u(|\bar{\mathbf{p}}-\bar{\mathbf{p}}'_1|,\eta)]^2. \tag{44}$$

Formally, the solution of Eq. (41) can be written as

$$\Phi = -\,(-i\,\bar{\omega}\Delta_0 + \mathscr{D} - \mathscr{I})^{-1}\,\frac{\{n_0,\delta U(r_0\bar{\mathbf{r}},\omega)\}}{(2N)^{\frac{1}{2}}}, \tag{45}$$

and the linear response can be determined using Eq. (40):

$$\langle O\rangle_t = \int d\Gamma \int \frac{d\omega}{2\pi}\,e^{-i\omega t}\,\Delta_0(\bar{p};\bar{r})\,\Phi(\bar{\mathbf{p}};\bar{\mathbf{r}},\omega^+)\,O(\mathbf{p};\mathbf{r}). \tag{46}$$

The difficulty is in inverting the operator appearing in the parentheses in Eq. (45). Decent approximate solutions, however, can be found using a variational technique known as the method of moments. To this end, we restrict the solution space of Eq. (41) to a subspace spanned by a set of basis functions of the phase-space variables $\{\phi_\alpha(\bar{\mathbf{p}};\bar{\mathbf{r}})\}$ (the "moments") and expand Φ and δU in this basis:

$$\begin{aligned}\Phi(\bar{\mathbf{p}};\bar{\mathbf{r}},\omega) &= \sum_\alpha \Phi_\alpha(\omega)\,\phi_\alpha(\bar{\mathbf{p}};\bar{\mathbf{r}}),\\ (2N)^{-\frac{1}{2}}\delta U(r_0\bar{\mathbf{r}},\omega) &= \sum_\alpha \delta U_\alpha(\omega)\,\phi_\alpha(\bar{\mathbf{p}};\bar{\mathbf{r}}).\end{aligned} \tag{47}$$

Plugging this ansatz into Eq. (41) and evaluating the moments of the resulting equation with respect to each of the basis functions, that is, multiplying the sides of the CBV equation by each of the basis functions and integrating over the phase-space variables, we find a closed set of linear equations for the coefficients $\{\Phi_\alpha\}$:

$$\begin{aligned}-i\bar{\omega}\langle\!\langle\phi_\beta\phi_\alpha\rangle\!\rangle\Phi_\alpha(\omega) + \langle\!\langle\phi_\beta\{\phi_\alpha,\bar{\mathcal{H}}_0\}\rangle\!\rangle\,[\delta U_\alpha(\omega) + \Phi_\alpha(\omega)]\\ + \langle\!\langle\phi_\beta\{\bar{\Sigma}[\Delta_0\phi_\alpha],\bar{\mathcal{H}}_0\}\rangle\!\rangle\Phi_\alpha(\omega) - \mathscr{I}_{\beta\alpha}\Phi_\alpha(\omega) = 0,\end{aligned} \tag{48}$$

where we have defined the "Δ_0 average" as

$$\langle\!\langle\mathcal{A}(\bar{\mathbf{p}};\bar{\mathbf{r}})\rangle\!\rangle \equiv \int d\bar{\Gamma}\;\Delta_0(\bar{\mathbf{p}};\bar{\mathbf{r}})\mathcal{A}(\bar{\mathbf{p}};\bar{\mathbf{r}}). \tag{49}$$

Summation over repeated indices is implied in Eq. (48). The matrix elements of the collision integral, $\mathscr{I}_{\alpha\beta} \equiv \int d\bar{\Gamma}\,\phi_\alpha\mathscr{I}[\phi_\beta]$ can be put in the following symmetric form using the symmetry properties of the collision integral kernel:

$$\begin{aligned}\mathscr{I}_{\alpha\beta} = -\frac{\bar{\beta}(2N)^{\frac{1}{2}}}{8}\int d^2\bar{\mathbf{r}}\int\frac{d^2\bar{\mathbf{p}}}{(2\pi)^2}\frac{d^2\bar{\mathbf{p}}_1}{(2\pi)^2}\frac{d^2\bar{\mathbf{p}}'}{(2\pi)^2}\frac{d^2\bar{\mathbf{p}}'_1}{(2\pi)^2}\\ \times(2\pi)\delta(\Delta\bar{E})\,(2\pi)^2\delta^2(\Delta\bar{\mathbf{P}})\,|\bar{\mathcal{M}}|^2\,\mathrm{S}[\phi_\alpha]\,\mathrm{S}[\phi_\beta]\\ \times n_0n_{0,1}(1-n'_0)(1-n'_{0,1}).\end{aligned} \tag{50}$$

The first term on the second line of Eq. (48) can be put in a more useful form using the identity $\phi_\beta\{\bar{\Sigma}[\Delta_0\phi_\alpha],\bar{\mathcal{H}}_0\} = \{\phi_\beta\bar{\Sigma}[\Delta_0\phi_\alpha],\bar{\mathcal{H}}_0\} - \bar{\Sigma}[\Delta_0\phi_\alpha]\{\phi_\beta,\bar{\mathcal{H}}_0\}$. Taking the Δ_0 average of both sides on this identity, the first term on the left-hand side vanishes. To see this, note that $\langle\!\langle\{\psi,\bar{\mathcal{H}}_0\}\rangle\!\rangle = \int d\bar{\Gamma}\,\Delta_0\{\psi,\bar{\mathcal{H}}_0\} = \int d\bar{\Gamma}\,\{\Delta_0\psi,\bar{\mathcal{H}}_0\}$ for arbitrary ψ. The last equality holds since $\{\Delta_0,\bar{\mathcal{H}}_0\} = 0$. Since $\Delta_0 \to 0$ exponentially fast for large $\bar{\mathbf{r}}$ or $\bar{\mathbf{p}}$, the Stokes' theorem implies that the last integral vanishes as long as ψ is exponentially bounded.

Here, $\psi = \phi_\beta \bar{\Sigma}[\Delta_0 \phi_\alpha]$, which is, in fact, exponentially bounded. Finally, Eq. (48) can be put in the following matrix form:

$$(-i\bar{\omega}\mathsf{M} + \mathsf{H}_0 - \Sigma - \mathsf{I}_c)\Phi(\omega) = -\mathsf{H}_0\,\delta\mathbf{U}(\omega), \tag{51}$$

where

$$\begin{aligned} (\mathsf{M})_{\alpha\beta} &= \langle\!\langle \phi_\alpha \phi_\beta \rangle\!\rangle, \\ (\mathsf{H}_0)_{\alpha\beta} &= \langle\!\langle \phi_\alpha \{\phi_\beta, \bar{\mathcal{H}}_0\} \rangle\!\rangle, \\ (\Sigma)_{\alpha\beta} &= \langle\!\langle \bar{\Sigma}[\Delta_0\phi_\beta]\{\phi_\alpha, \bar{\mathcal{H}}_0\} \rangle\!\rangle, \\ (\mathsf{I}_c)_{\alpha\beta} &= \mathscr{I}_{\alpha\beta}, \end{aligned} \tag{52}$$

and $\Phi(\omega)$ and $\delta\mathbf{U}(\omega)$ are the vectors with entries $\Phi_\alpha(\omega)$ and $\delta U_\alpha(\omega)$, respectively. If the observable $O(\bar{\mathbf{p}};\bar{\mathbf{r}})$ is also expressible in terms of the basis functions, $O(\bar{\mathbf{p}};\bar{\mathbf{r}}) = \sum_\alpha O_\alpha \phi_\alpha(\bar{\mathbf{p}};\bar{\mathbf{r}})$, then the linear response can be conveniently written as

$$\begin{aligned} \langle O \rangle_\omega &= \int d\bar{\Gamma}\; O_\beta \phi_\beta\; \Delta_0 \Phi_\alpha(\omega^+)\phi_\alpha \\ &= \mathbf{O}^T \mathsf{M}\, \Phi(\omega^+). \end{aligned} \tag{53}$$

Equations (51)–(53) are similar to the analysis of Ref. [35]. Here, however, we have an additional matrix Σ that accounts for the residual mean-field due to self-consistency.

It is useful to define an "evolution matrix" and express it in its diagonal basis:

$$\mathsf{E} \equiv \mathsf{M}^{-1}(\mathsf{H}_0 - \Sigma - \mathsf{I}_c) = i\,\mathsf{V}\Omega\mathsf{V}^{-1}, \tag{54}$$

where Ω is the diagonal matrix of eigenvalues and V is the matrix of eigenvectors. Note that, in general, E is a not a Hermitian matrix and may have complex eigenvalues. Moreover, it is a non-normal matrix and therefore, its eigenvectors are not orthogonal [37]. Using the diagonal form of the evolution matrix, Eq. (51) can be expressed as

$$\Phi(\omega) = -i\mathsf{V}\,\frac{1}{\omega - \Omega}\,\mathsf{V}^{-1}\mathsf{M}^{-1}\mathsf{H}_0\,\delta\mathbf{U}(\omega). \tag{55}$$

The real and imaginary parts of Ω determine the oscillation frequency and damping of the eigenmodes. Clearly, not all of the eigenmodes are expected to contribute to the linear response to a given perturbation. This becomes particularly important when one is dealing with a large variational basis set. In such cases, as we will see later, the evolution matrix will have poles which are very close to each other on the complex frequency plane and it is not *a priori* clear which one(s) and the proportion to which it (they) contributes to the response of the system. Using the linear response formalism described here, however, this question does not need to be addressed separately. Using Eqs. (53) and (55), we get

$$\begin{aligned} \langle O \rangle_\omega &= \sum_\alpha \frac{r_\alpha(\omega)}{\omega - \Omega_\alpha}, \\ r_\alpha(\omega) &= -i[\mathsf{V}^T\mathsf{M}\mathbf{O}]_\alpha [\mathsf{V}^{-1}\mathsf{M}^{-1}\mathsf{H}_0\,\delta\mathbf{U}(\omega)]_\alpha; \end{aligned} \tag{56}$$

that is, the residues r_α can be expressed in terms of the known matrices. Note that in case of Dirac δ perturbations, $\delta\mathbf{U}(\omega)$ is independent of ω and so are the residues.

Before we attempt to obtain accurate solutions obtained using large variational basis sets, we find it useful to make simple analytical predictions using a small basis set as the first step. We use the scaling ansatz approach to find such a basis set and neglect self-energy corrections to simplify the calculations at first. We extend the basis set and include self-energy corrections later and discuss the nature and importance of the corrections that follow.

V. LINEARIZED SCALING ANSATZ ANALYSIS

The scaling ansatz provides a simple and intuitive picture of the collective excitations of confined gases. This method has been applied to various systems in both isotropic and anisotropic traps, including Bose gases below and above the critical temperature, s-wave and dipolar fermions in the CL and HD regimes [22–27,30]. Here, we apply the method to the CBV equation, which, as we shall see, allows us to study both CL and HD limits as well as transition from one regime to the other.

In this method, one assumes that the nonequilibrium quasiparticle distribution function can be approximately described as a scaled copy of the equilibrium distribution:

$$n_{\mathrm{SA}}(\bar{\mathbf{p}};\bar{\mathbf{r}},t) \equiv \frac{1}{\prod_i (b_i\phi_i)}\, n_0\big[\phi_i^{-1}(\bar{p}_i - \dot{b}_i\bar{r}_i/b_i); \bar{r}_i/b_i\big], \tag{57}$$

where b_i and ϕ_i $(i = x,y)$ are time-dependent scale factors of positions and momenta. The prefactor is to ensure conservation of particle number. The equilibrium solution corresponds to the choice $b_x = b_y = \phi_x = \phi_y = 1$. Introducing reparametrization of the scaling variables

$$\begin{aligned} b_x(t) &= 1 + \bar{\lambda}(t) + \lambda(t), \quad b_y(t) = 1 + \bar{\lambda}(t) - \lambda(t), \\ \phi_x(t) &= 1 + \bar{\nu}(t) + \nu(t), \quad \phi_y(t) = 1 + \bar{\nu}(t) - \nu(t), \end{aligned} \tag{58}$$

and expanding Eq. (57) to first order in λ, $\bar{\lambda}$, ν, and $\bar{\nu}$, we get

$$\begin{aligned} \delta n_{\mathrm{SA}} \approx -2(\bar{\lambda} + \bar{\nu})n_0 + \Delta_0[\dot{\bar{\lambda}}\,\bar{\mathbf{r}}\cdot\bar{\mathbf{p}} + \bar{\nu}\,\bar{p}^2 + \bar{\lambda}\,\bar{r}^2] \\ + \Delta_0\big[\dot{\lambda}\,(\bar{x}\bar{p}_x - \bar{y}\bar{p}_y) + \nu\,(\bar{p}_x^2 - \bar{p}_y^2) + \lambda\,(\bar{x}^2 - \bar{y}^2)\big], \end{aligned} \tag{59}$$

where $\delta n_{\mathrm{SA}} \equiv n_{\mathrm{SA}} - n_0$. We have neglected self-energy corrections to simplify the analysis and explicitly used the noninteracting equilibrium solution. Also, $\Delta_0 = \partial n_0/\partial\bar{\mu} = \bar{\beta}n_0(1 - n_0)$ as before. Here, $(\bar{\lambda},\bar{\nu})$ and (λ,ν) control the isotropic (monopole) and anisotropic (quadrupole) scalings. Comparing the last equation to Eq. (40), we can recognize the first and second set of terms in the brackets as Φ_{mon} and Φ_{quad}, that is, the variational basis set that the scaling ansatz provides for monopole and quadrupole modes, respectively.

The first term in Eq. (59), which is a consequence of the normalization prefactor of the scaling ansatz requires further discussion. First of all, we note that this term may only be nonvanishing in the monopole case. Since quadrupole oscillations are purely anisotropic, none of the terms appearing in Φ_{quad} violate the conservation of mass in the linear regime and therefore no normalization is necessary. The monopole oscillations as described by Φ_{mon}, however, may violate the conservation of mass and the ansatz must be fixed with

a counterterm. The scaling ansatz fixes this defect with a uniform scaling of the distribution, leading to the first term in Eq. (59). Unless one restricts the ansatz by setting $\phi_i^{-1} = b_i$ (so that $\bar{\lambda} + \bar{\nu} = 0$), the ansatz may lead to unphysical conclusions once collisions are taken into account. It is generally understood that the nonequilibrium dynamics of degenerate Fermi gases are governed by excitations near the Fermi surface while the fermions deep inside the Fermi sea remain in place due to their large excitation energy gap. A global rescaling of the quasiparticle distribution, that is, a uniform rescaling of quasiparticle occupations irrespective of their energy gap implies mobilization of all particles with the same likelihood, including those which are deep inside the Fermi sea. This is clearly an unphysical picture and may lead to unrealistically large collision rates.

To address this issue, we remove the global normalization factor and allow the chemical potential to vary instead. This amounts to adding a term $\sim\delta\bar{\mu}(t)\,\partial n_0/\partial\bar{\mu} = \Delta_0\,\delta\mu(t)$ to the ansatz, that is, adding $\phi = 1$ to the monopole basis set. The phase-space moment equation that is associated with this trivial moment function is exactly the statement of conservation of mass. In summary, we obtain

$$\Phi_{\rm mon} = \delta\mu(t) + c_1(t)\,\bar{\mathbf{r}}\cdot\bar{\mathbf{p}} + c_2(t)\,\bar{r}^2 + c_3(t)\,\bar{p}^2 \qquad (60)$$

and

$$\Phi_{\rm quad} = d_1(t)\,(\bar{x}\,\bar{p}_x - \bar{y}\,\bar{p}_y) + d_2(t)(\bar{x}^2 - \bar{y}^2) + d_3(t)(\bar{p}_x^2 - \bar{p}_y^2), \qquad (61)$$

where $\delta\mu(t)$, $c_i(t)$, and $d_i(t)$ are time-dependent functions to be determined.

The determination of these unknown functions is usually done by plugging the ansatz into the kinetic equation, multiplying the resulting equation by each of the basis functions and integrating over the phase-space variables to obtain a close set of differential equations. This is equivalent to the formalism described in Sec. IV and we prefer to do it in our matrix notation as a warmup for the later sections, where we extend the basis set and include self-energy corrections. We remark that the role of various terms appearing in Eqs. (60) and (61) can be understood intuitively. In particular, $\bar{\mathbf{r}}\cdot\bar{\mathbf{p}}$ and $\bar{x}\,\bar{p}_x - \bar{y}\,\bar{p}_y$ in $\Phi_{\rm mon}$ and $\Phi_{\rm quad}$ correspond to isotropic and anisotropic scaling velocity fields $\mathbf{v}_{\rm mon} \propto \bar{\mathbf{r}}$ and $\mathbf{v}_{\rm quad} \propto \bar{x}\mathbf{e}_x - \bar{y}\mathbf{e}_y$.

A. Monopole oscillations from the scaling ansatz

Neglecting self-energy corrections, we get $\Sigma = 0$, and $\bar{\mathcal{H}}_0 = (\bar{r}^2 + \bar{p}^2)/2$ using which we can easily calculate M and H_0. The collision matrix elements identically vanish due to conservation of energy and momentum [see Eq. (50), and notice that $\mathrm{S}[1] = \mathrm{S}[\bar{r}^2] = 0$, $\mathrm{S}[\bar{p}^2] = 2\Delta\bar{E}$ and $\mathrm{S}[\bar{\mathbf{r}}\cdot\bar{\mathbf{p}}] = \bar{\mathbf{r}}\cdot\Delta\bar{\mathbf{P}}$]. While it is possible to find analytic expressions for the Δ_0 averages appearing in M and H_0, we find that they all factor out from the evolution matrix using the relations $\langle\!\langle\bar{r}^2\rangle\!\rangle = \langle\!\langle\bar{p}^2\rangle\!\rangle$ and $\langle\!\langle\bar{r}^4\rangle\!\rangle = \langle\!\langle\bar{p}^4\rangle\!\rangle$ we have here. The evolution matrix evaluates to the following simple form

$$\mathsf{E}_{\rm SA}^{\rm mon} = \begin{pmatrix} 0 & 0 & 0 & 0 \\ 0 & 0 & 2 & -2 \\ 0 & -1 & 0 & 0 \\ 0 & 1 & 0 & 0 \end{pmatrix} \qquad (62)$$

and is independent of temperature. In the above equation, the matrix elements appear in the same order as the basis functions in Eq. (60). The monopole excitation operator is r^2, which gives the "excitation vector" $\delta\mathbf{U} = (0,0,1,0)^T$ in the scaling ansatz basis [see the definition of $\delta\mathbf{U}$ after Eq. (52)]. Using Eq. (55), we finally find

$$\Phi_{\rm mon}(\bar{\mathbf{p}};\bar{\mathbf{r}},\omega) = [-2i\bar{\omega}(\bar{\mathbf{r}}\cdot\bar{\mathbf{p}}) + 2\bar{r}^2 - 2\bar{p}^2]/(\bar{\omega}^2 - 4). \qquad (63)$$

The frequency of oscillations is given by the poles of the denominator, $\bar{\omega}_{\rm mon} = \pm 2$, which is a well-known result [32]. We state it without proof that extending the monopole basis has no effect on this result as long as self-energy corrections are neglected. In fact, it is a well-known fact that the full nonlinear Boltzmann equation (including collisions) admits an exact monopole solution with frequency $2\omega_0$ [32], corresponding to a nodeless scaling velocity field $\propto\mathbf{r}$. The existence of this undamped solution is deeply related to the fact that the trap potential is harmonic and the particles are assumed to have quadratic dispersions. Using dressed quasiparticle dispersions or adding an anharmonicity to the trap potential both lead to the violation of this exact result.

We remark that besides the $\bar{\omega} = \pm 2$, the above evolution matrix admits two zero eigenvalues that correspond to eigenvector $\Phi \sim 1$ and $\Phi \sim \bar{r}^2 + \bar{p}^2$. Both of these eigenvectors correspond to unphysical excitations since they violate conservation of mass. However, it is easy to see that both lie in the null space of $\mathsf{H}_{0,\rm SA}^{\rm mon}$. Therefore, using Eq. (55), we see that these unphysical modes will never be excited regardless of one's choice of excitation vector $\delta\mathbf{U}$. The number of such unphysical modes increases as one extends the variational basis set.

B. Quadrupole oscillations from the scaling ansatz

We find the following forms for M and H_0 in the quadrupole basis:

$$\mathsf{M}_{\rm SA}^{\rm quad} = \frac{1}{2}\begin{pmatrix} \langle\!\langle\bar{r}^2\bar{p}^2\rangle\!\rangle & 0 & 0 \\ 0 & \langle\!\langle\bar{r}^4\rangle\!\rangle & 0 \\ 0 & 0 & \langle\!\langle\bar{p}^4\rangle\!\rangle \end{pmatrix} \qquad (64)$$

and

$$\mathsf{H}_{0,\rm SA}^{\rm quad} = \frac{1}{2}\begin{pmatrix} 0 & 2\langle\!\langle\bar{r}^2\bar{p}^2\rangle\!\rangle & -2\langle\!\langle\bar{r}^2\bar{p}^2\rangle\!\rangle \\ -\langle\!\langle\bar{r}^4\rangle\!\rangle & 0 & 0 \\ -\langle\!\langle\bar{p}^4\rangle\!\rangle & 0 & 0 \end{pmatrix}. \qquad (65)$$

The order of basis functions is the same as it appears in Eq. (61). The only nonzero collision matrix element is $\mathscr{I}_{33}$, the rest of which vanish again due to conservation laws [see Eq. (50), and note that $\mathrm{S}[\bar{x}^2 - \bar{y}^2] = 0$ and $\mathrm{S}[\bar{x}\,\bar{p}_x - \bar{y}\,\bar{p}_y] = (\bar{x}\mathbf{e}_x - \bar{y}\mathbf{e}_y)\cdot\Delta\bar{\mathbf{P}}$]. The collision integral can be expressed as follows using the results of Appendixes C4 and D4

[in particular, see Eq. (C20)]:

$$\mathscr{I}_{33}^{\text{quad}} = -64\pi(2N)^{\frac{1}{2}}\lambda_d^2\,\bar{T}^5\int_0^\infty \rho^5\,d\rho\int_0^{2\pi}\frac{d\phi}{2\pi}\int_0^{2\pi}\frac{d\phi'}{2\pi}\int_0^{\frac{\pi}{2}} d\xi\,\sin^7\xi\,\cos\xi\int_0^{\frac{\pi}{2}} d\nu\,\sin^5\nu\,\cos\nu$$
$$\times\,\sin^2(\phi-\phi')[\chi_1\,\text{Erfcx}(2\eta\chi_1\sqrt{\bar{T}\rho}) - \chi_2\,\text{Erfcx}(2\eta\chi_2\sqrt{\bar{T}\rho})]^2$$
$$\times\left[\frac{1}{\cosh(\rho-\bar{\mu}/\bar{T})+\cosh(\rho\,\sin^2\xi\,\sin 2\nu\cos\phi)}\,\frac{1}{\cosh(\rho-\bar{\mu}/\bar{T})+\cosh(\rho\,\sin^2\xi\,\sin 2\nu\cos\phi')}\right], \tag{66}$$

where $\chi_1 = \sin\xi\,\sin\nu\,|\sin[(\phi-\phi')/2]|$ and $\chi_2 = \sin\xi\,\sin\nu\,|\cos[(\phi-\phi')/2]|$. The above integration cannot be carried out analytically in general and requires a numerical treatment. The analytical low-T and high-T asymptotic results are given in Appendix B. Note that the (dimensionless) noninteracting chemical potential $\bar{\mu}$ is given implicitly by Eq. (34) and only depends on the dimensionless temperature $\bar{T}$. Therefore, except for the prefactor, the above integral is a universal function of $\bar{T}$ and η. We define the dimensionless "quadrupole collision rate" ν_c as

$$\nu_c \equiv -\frac{2\mathscr{I}_{33}^{\text{quad}}}{\langle\langle\bar{p}^4\rangle\rangle} \equiv N\left(\frac{a_d}{a_0}\right)^2 Q(\bar{T},\eta). \tag{67}$$

The last equation also serves as the definition of the universal function $Q(\bar{T},\eta)$. The quadrupole excitation operator is x^2-y^2, which yields $\delta\mathbf{U}=(0,1,0)^T$ in this basis and, finally, a simple calculation similar to the monopole case yields

$$\Phi_{\text{quad}}(\bar{\mathbf{p}};\bar{\mathbf{r}},\omega) = \big[2\bar{\omega}(\nu_c - i\bar{\omega})(\bar{x}\,\bar{p}_x - \bar{y}\,\bar{p}_y) + 2i(\nu_c - i\bar{\omega})$$
$$\times(\bar{x}^2-\bar{y}^2) + 2\bar{\omega}\big(\bar{p}_x^2-\bar{p}_y^2\big)\big]/\mathfrak{D}_{\text{quad}}(\bar{\omega},\nu_c), \tag{68}$$

where $\mathfrak{D}_{\text{quad}}(\bar{\omega},\nu_c)$ is the quadrupole characteristic equation and is given by

$$\mathfrak{D}_{\text{quad}}(\bar{\omega},\nu_c) = \bar{\omega}(\bar{\omega}^2-4) + i\,\nu_c(\bar{\omega}^2-2). \tag{69}$$

The roots of $\mathfrak{D}_{\text{quad}}(\bar{\omega},\nu_c)$ determine the frequency and damping of quadrupole oscillations. We note that Eq. (68), along with the characteristic equation given above, are "generic" results in the sense that one obtains the same expression for quadrupole oscillations independent of the specific form of interactions. For instance, Refs. [31] and [38] obtain the same characteristic equation for s-wave fermions and a classical gas, respectively. The model-specific details are encoded in the collision rate ν_c. Therefore, it is worthwhile to review the generic features of the quadrupole oscillations from Eq. (68) in terms of ν_c as a first step. We return to the analysis of ν_c afterwards.

Two important limits can be recognized for quadrupole oscillations. The CL limit is achieved for $\nu_c \to 0$:

$$\lim_{\nu_c\to 0}\Phi_{\text{quad}}(\bar{\mathbf{p}};\bar{\mathbf{r}},\omega) \equiv \Phi_{\text{quad}}^{\text{CL}}(\bar{\mathbf{p}};\bar{\mathbf{r}},\omega) = \big[-2i\bar{\omega}(\bar{x}\,\bar{p}_x - \bar{y}\,\bar{p}_y)$$
$$+2(\bar{x}^2-\bar{y}^2) - 2\big(\bar{p}_x^2-\bar{p}_y^2\big)\big]/(\bar{\omega}^2-4). \tag{70}$$

Notice the formal similarity to the monopole case. In this limit, we obtain undamped oscillations at $\omega_{\text{quad}}^{\text{CL}} = 2\omega_0$ which correspond to the free motion of particles in the trap. In the limit of very fast collisions, $\nu_c \to \infty$, we find

$$\lim_{\nu_c\to\infty}\Phi_{\text{quad}}(\bar{\mathbf{p}};\bar{\mathbf{r}},\omega) \equiv \Phi_{\text{quad}}^{\text{HD}}(\bar{\mathbf{p}};\bar{\mathbf{r}},\omega) = [-2i\bar{\omega}(\bar{x}\,\bar{p}_x$$
$$-\bar{y}\,\bar{p}_y) + 2(\bar{x}^2-\bar{y}^2)]/(\bar{\omega}^2-2), \tag{71}$$

which describes undamped oscillations at a frequency $\omega_{\text{quad}}^{\text{HD}} = \sqrt{2}\omega_0$. This is the well-known quadrupole "surface" mode which is also obtained by solving ideal HD equations for harmonically trapped gases [33]. Although we have neglected self-energy corrections here, it can be shown that the frequencies of these HD modes are universal since they do not change the density in the bulk, are confined to the surface, and are entirely driven by the trap restoring force [33]. We observe this universality in later sections, where we include self-energy corrections and still obtain the same oscillation frequency in the HD limit.

Except for the two ideal limits discussed so far, quadrupole oscillations are otherwise damped for any finite value of ν_c. For large nu_c (near HD), this is due to the fact that the collisions are not fast enough to maintain the local equilibrium and thus lead to dissipation. For small ν_c (near CL), collisions result in a friction between the otherwise freely moving particles and again lead to dissipation. In general, the oscillation frequency and damping rate can be found by analyzing the roots $\mathfrak{D}_{\text{quad}}(\bar{\omega},\nu_c)$. Figures 5(a)–5(c) show the real and imaginary parts of the poles as a function of ν_c. In the limit $\nu_c \ll 1$, the three poles are approximately located at

$$\pm\left(2-\frac{5\nu_c^2}{64}\right) - \frac{i\,\nu_c}{4} + O\big(\nu_c^5\big), \quad -\frac{i\,\nu_c}{2} + i\,O\big(\nu_c^3\big). \tag{72}$$

The first two poles describe a damped oscillatory mode at a frequency slightly lower than $2\omega_0$ and a damping rate of $\sim\nu_c\omega_0/2$. The third pole corresponds to an overdamped component. In the other limit $\nu_c \gg 1$, we get

$$\pm\left(\sqrt{2}+\frac{3}{2\sqrt{2}\nu_c^2}\right) - \frac{i}{\nu_c} + O\big(\nu_c^{-3}\big), \quad -i\,\nu_c + i\,O\big(\nu_c^{-1}\big). \tag{73}$$

Again, the first two poles describe a damped oscillatory mode at a frequency slightly higher than $\sqrt{2}\omega_0$ and a damping rate of $\sim\nu_c^{-1}\omega_0$, accompanied by a (highly) overdamped component with a damping rate of $\omega_0\nu_c$. Studying the residues of the overdamped poles, we find that the contribution of the this component is $\propto\nu_c^2$ and $\propto\nu_c^{-2}$ to leading order in the CL and HD limits, respectively, and has its maximum contribution in the CL-HD crossover regime. We associate the presence

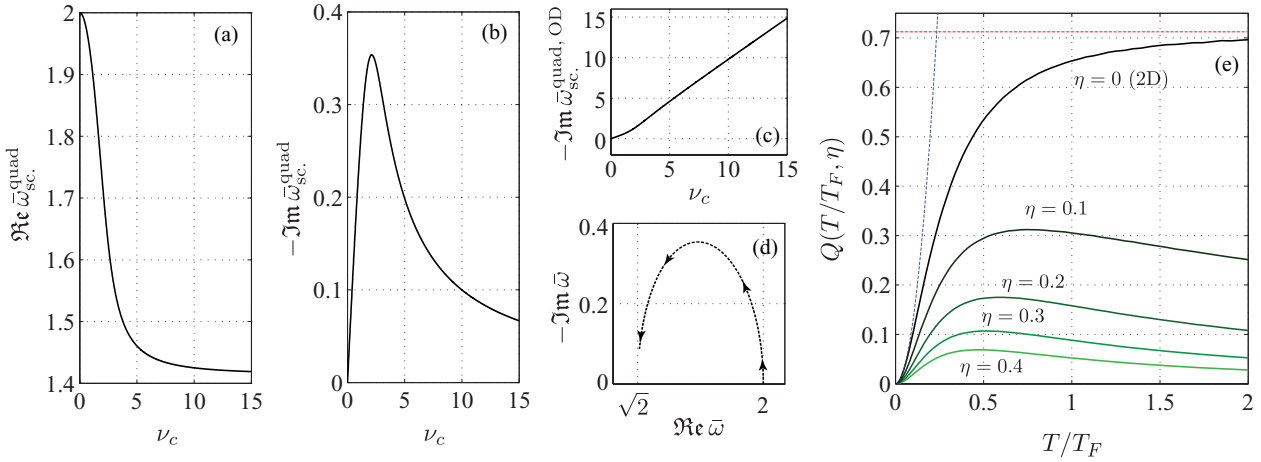

FIG. 5. (Color online) Frequency and damping of quadrupole oscillations of quasi-2D dipolar fermions in isotropic harmonic traps from the scaling ansatz analysis. (a), (b) The frequency and damping of oscillations vs ν_c, respectively. (c) The damping rate of the overdamped component vs ν_c. (d) The evolution of the damped oscillatory pole on the complex plane upon increasing ν_c in the range [0,15]. (e) $Q(T/T_F,\eta)$ as a function of T/T_F for different values of $\eta \equiv (2N)^{\frac{1}{4}}(\omega_0/\omega_z)^{\frac{1}{2}}$. Q is related to the quadrupole collision rate as $\nu_c = N(a_d/a_0)^2\, Q(T/T_F,\eta)$. The low-temperature and high-temperature asymptotes in the 2D limit are shown as blue and red (horizontal) dashed lines, respectively.

of such an overdamped component to the initial high-energy excitations. Figure 5(d) shows the evolution of the first pole on the complex frequency plane upon increasing ν_c: It starts off on $2\omega_0$, moves to the lower half plane, and finally returns to the real axis at the HD frequency $\sqrt{2}\omega_0$.

We finally turn to the analysis of $Q(\bar{T},\eta)$, the universal function that controls the quadrupole collision rate ν_c for dipole-dipole interactions [Eq. (67)]. ν_c can be identified with different quantities in different regimes. In the collision-dominated regime (i.e., $\nu_c \gg 1$) where a viscous HD description is admissible, the shear viscosity sum rule yields ν_c as $\omega_0\langle P/\eta_s\rangle_{\rm trap}$, where P, η_s, and ω_0 are the local pressure, shear viscosity, and the trap frequency, respectively [15]. By $\langle\cdots\rangle_{\rm trap}$, we imply averaging over the trap. In the classical regime ($T \gg T_F$), one finds $\nu_c \sim \tau_c^{-1}$, where τ_c is the typical time between two single-particle collisions [31]. This can be established by replacing the Fermi-Dirac with Boltzmann-Maxwell distribution and evaluating the collision integral in the saddle-point approximation.

We have calculated Q for several values of η as a function of $\bar{T}$ by evaluating the 5D integral appearing in Eq. (66) numerically. The results are shown in Fig. 5(e). The asymptotic behavior of Q can be found analytically in the low- and high-temperature regimes and is given in Appendix B in the 2D limit ($\eta = 0$). They appear on the same figure as red and blue dashed lines. We find that $Q \sim \bar{T}^2$ for small T, while it saturates to a constant value for large $\bar{T}$. The low-temperature T^2 scaling is related to Pauli blocking; however, it is different from the case of 2D s-wave fermions (and 2D paramagnetic electron gas), where one finds $\nu_c \sim T^2\,\ln(T/T_F)^{-2}$ [15,39]. This difference can be traced back to the fact that the system investigated here is spin polarized and the s-wave scattering channel is blocked. The logarithmic enhancement of the shear viscosity (i.e., attenuation of ν_c) originates from the logarithmic divergence of the s-wave scattering length in the near-threshold regime in 2D. We remark that the near-threshold cross section of all other scattering channels remains bounded [29], leading to a bounded Born cross section.

The high-temperature plateau is a unique feature of near-threshold dipole-dipole scatterings in the 2D limit and its existence can be understood in terms of the interplay between the temperature dependence of the scattering cross section and rarefaction of the gas. Provided that $T_F \ll T \ll T_{\rm dip}$, we can estimate the relaxation rate using the aforementioned identification $\nu_c \sim \tau_c^{-1}$. The Born 2D scattering cross section scales like $\sigma_{\rm B} \sim q^{-1}|\tilde{\mathcal{V}}(q)|^2 \sim q a_d^2\,{\rm Erfcx}^2(q a_z)$, where q is the typical momentum of scattering particles and is $\sim(m k_B T)^{1/2}$ in the high-temperature regime. The collision frequency is $\tau_c^{-1} \sim \hbar q l_{\rm mfp}^{-1} \equiv \hbar q n \sigma$, where $l_{\rm mfp} = (n\sigma)^{-1}$ is the mean free path. The density at the center of the trap is $n_0 = m\omega_0^2 N/(2\pi T)$ and decreases as $1/T$. Combining these results, the collision rate amounts to

$$\nu_c \sim N\left(\frac{a_d}{a_0}\right)^2 {\rm Erfcx}^2\left[\left(\frac{k_B T}{\hbar\omega_z}\right)^{\frac{1}{2}}\right], \quad (T_F \ll T \ll T_{\rm dip}). \tag{74}$$

In the $2D$ limit, $\omega_z \to \infty$ and we find $\nu_c = {\rm const}$ [note that ${\rm Erfcx}(0) = 1$]. In other words, the growth of scattering cross section counteracts rarefaction of the gas to yield a constant collision rate. For finite ω_z, the scattering cross section starts to decrease once $k_B T \gtrsim \hbar\omega_z$ and, consequently, ν_c decays like $\sim 1/T$ [note that ${\rm Erfcx}(x) \sim 1/x$ for large x]. We remark that the single subband picture adopted here is no longer valid in the quasi-2D regime for $k_B T \gtrsim \hbar\omega_z$ and one must take into account the higher subbands as well. We have shown in a previous paper [40] that all intersubband interaction matrix elements have the same long wavelength behavior and therefore, we expect this scaling result to remain unaffected.

The plateau reached in the 2D limit relies crucially on the applicability of the Born approximation. As mentioned earlier, the scatterings enter the semiclassical regime for $T \gtrsim T_{\rm dip}$ [see Eq. (25)] and Born approximation breaks down. In this regime, the total scattering cross section can be estimated using the Eikonal approximation [28] and one finds $\sigma_{\rm SC} \sim (a_d/q)^{1/2}$. Repeating the same analysis with the semiclassical cross

section, we find

$$v_c \sim N \left(\frac{a_d}{a_0}\right)^{\frac{1}{2}} \left(\frac{\hbar\omega_0}{k_B T}\right)^{\frac{3}{4}}, \quad (T \gtrsim T_{\rm dip}). \tag{75}$$

The qualitative behavior of v_c for the full range of temperatures was shown earlier in Fig. 1(b1).

So far, we have neglected self-energy corrections in the description of the collective modes. We have also restricted our analysis to a variational calculation within a small basis set. In the next section, we extend our analysis to address both of these shortcomings.

VI. EXTENDED BASIS ANALYSIS: THE EFFECT OF HIGHER-ORDER MOMENTS AND SELF-ENERGY CORRECTIONS

The general formalism described in Sec. IV allows one to include self-energy corrections and to obtain a more accurate calculation of the response functions by extending the variational basis set in a controlled way. Using simple symmetry considerations, we introduce extensible polynomial-like variational basis sets relevant for describing monopole and quadrupole dynamics. Finite truncations of these basis sets allows one to satisfy all phase-space moments of the CBV equation up to the truncation order. Since we are dealing with large basis sets and self-energy corrections at finite temperatures, resorting to numerical methods is inevitable at this stage and no simple analytic results are expected to be found.

Our goal here is to evaluate the linear responses accurately within the approximations made so far. In practice, the reliability of the approximate linear response functions obtained using the method of moments depends on one's choice of the basis functions. This choice can be motivated by the symmetries of the perturbing potential and the equilibrium state. Here, the trap potential is assumed to be isotropic and it is easy to see that $[\mathscr{D}, L_z] = [\mathscr{I}, L_z] = 0$, where $L_z \equiv L_z^{(r)} + L_z^{(p)}$, $L_z^{(r)} = i(x\partial_y - y\partial_x)$, and $L_z^{(p)} = i(p_x\partial_{p_y} - p_y\partial_{p_x})$ are the rotation operators in the coordinate and momentum space, respectively. Therefore, if δU lies in a certain eigenspace of L_z; so will the solution of the linearized equation Φ and one may choose the basis functions from the same eigenspace. Another symmetry which is preserved by the CBV equation is the reflection symmetry. Defining the x-reflection operator as $R_x\phi(p_x,p_y;x,y) = \phi(-p_x,p_y;-x,y)$, it is easy to show that the linearized evolution operator commutes with R_x as well. We utilize these observations to define appropriate (and extensible) basis sets for monopole and quadrupole dynamics in the next two sections.

A. Variational basis set for monopole oscillations

The generator of monopole oscillations, $\delta U_m \sim r^2$, belongs to the zero-angular-momentum representation of L_z. An arbitrary function of such type can be expressed as $f(p,r)[(x+iy)(p_x - ip_y)]^n$ for $n \in \mathbb{Z}$ and arbitrary $f(p,r)$. Any smooth function of this type can be written as a power series expansion in r^2, p^2, $\mathbf{r}\cdot\mathbf{p}$, and $\xi \equiv yp_x - xp_y$. Observing that $\xi^2 = r^2p^2 - (\mathbf{r}\cdot\mathbf{p})^2$, the most general basis for such functions can be constructed from the following two classes:

$$\begin{aligned}\phi_\alpha^+ &\equiv \phi_{(m_\alpha,n_\alpha,k_\alpha)} = r^{2m_\alpha}\, p^{2n_\alpha} (\mathbf{r}\cdot\mathbf{p})^{k_\alpha},\\ \phi_\alpha^- &\equiv \phi_{(m_\alpha,n_\alpha,k_\alpha)} = \xi\, r^{2m_\alpha}\, p^{2n_\alpha} (\mathbf{r}\cdot\mathbf{p})^{k_\alpha}.\end{aligned} \tag{76}$$

Observing that $R_x\phi_\alpha^\pm = \pm\phi_\alpha^\pm$ and the fact that the equilibrium state and the perturbations are reflection symmetric, we discard $\{\phi_\alpha^-\}$. We define $\{\phi_\alpha^+\}$ as the "extended monopole basis" and drop the $+$ superscript for brevity. To truncate the basis set, we keep all basis functions satisfying $m+n+k \leqslant M$, where M is a positive integer which we call the order of the basis set. A first-order basis set contains four elements, $\{1, \mathbf{r}\cdot\mathbf{p}, p^2, r^2\}$ and is equivalent to the linearized scaling ansatz discussed earlier. In general, a basis set of order M has $(M+1)(M+2)(M+3)/6$ elements. Expressions useful for numerical evaluation of the matrix elements of M, H_0, Σ, and I_c in the monopole basis are given in Appendix C.

B. Variational basis set for quadrupole oscillations

By definition, a quadrupole (d-wave) function in 2D changes sign upon a simultaneous $\pi/2$ rotation of both $\mathbf{r}$ and $\mathbf{p}$. Such functions belong to the $m_z = \pm 2$ representation of L_z which can be expressed as $f(p,r)\, e^{iM\phi_r}\, e^{iN\phi_p}$, where M and N are two integers such that $M - N = \pm 2$, ϕ_r and ϕ_p are the angles $\mathbf{r}$ and $\mathbf{p}$ make with a fixed axis (we arbitrarily choose the x axis), and $f(p,r)$ is an arbitrary scalar function of $\mathbf{p}$ and $\mathbf{r}$. One can identify 12 classes of functions with such symmetry. Apart from the arbitrary scalar function $f(p,r)$, the accompanying multipliers can be

$$\begin{aligned}&\xi_1^+ \equiv x^2 - y^2, \quad \xi_2^+ \equiv p_x^2 - p_y^2, \quad \xi_3^+ \equiv xp_x - yp_y,\\ &\eta_1^+ \equiv xy(yp_x - xp_y), \quad \eta_2^+ \equiv p_x p_y (yp_x - xp_y),\\ &\eta_3^+ \equiv (yp_x + xp_y)(yp_x - xp_y),\end{aligned}$$

and

$$\begin{aligned}&\xi_1^- \equiv xy, \quad \xi_2^- \equiv p_x p_y, \quad \xi_3^- \equiv yp_x + xp_y,\\ &\eta_1^- \equiv (yp_x - xp_y)(x^2 - y^2), \quad \eta_2^- \equiv (yp_x - xp_y)\left(p_x^2 - p_y^2\right),\\ &\eta_3^- \equiv (yp_x - xp_y)(xp_x - yp_y).\end{aligned}$$

The functions with $+$ and $-$ superscript are even and odd eigenfunctions of the reflection operator R_x, respectively. Like before, we drop the second class. Also, we find the following relations between these prefactors:

$$\begin{aligned}2\eta_1^+ &= r^2\xi_3^+ - (\mathbf{r}\cdot\mathbf{p})\,\xi_1^+,\\ 2\eta_2^+ &= (\mathbf{r}\cdot\mathbf{p})\,\xi_2^+ - p^2\,\xi_3^+,\\ 2\eta_3^+ &= r^2\,\xi_2^+ - p^2\,\xi_1^+,\end{aligned} \tag{77}$$

using which we can drop the class of functions $f(p,r)\,\eta_i^+$ from the basis set. Since $f(p,r)$ is assumed to be a smooth scalar function of $\mathbf{p}$ and $\mathbf{r}$, it can be expanded in the monopole basis. Thus, in summary, we find that any smooth reflection symmetric quadrupolar function can be expanded in terms of $\{\xi_i^+\,\phi_\alpha^+\}$ for $i = 1,2,3$ and $\alpha = (m,n,k)$, where m, n, and k are non-negative integers and ϕ_α^+ are the previously introduced monopole basis functions. We denote this basis set as the "extended quadrupole basis." We also remark that this basis set can be reduced further in light of the relation

$2(\mathbf{r}\cdot\mathbf{p})\,\xi_2^+ = p^2\xi_1^+ + r^2\xi_3^+$, so that the basis functions of the type $\xi_2^+ r^{2m} p^{2n}(\mathbf{r}\cdot\mathbf{p})^{k+1}$ can be written as a linear combination of $\xi_1^+ r^{2m} p^{2n+2}(\mathbf{r}\cdot\mathbf{p})^k$ and $\xi_3^+ r^{2m+2} p^{2n}(\mathbf{r}\cdot\mathbf{p})^k$. Like before, we drop the $+$ superscript for brevity in the remainder of the paper. An order-M truncation of the quadrupole basis set is the finite set that comprises all quadrupole basis functions satisfying $k+m+n \leqslant M-1$. The first-order basis set contains three elements $\{x^2-y^2, p_x^2-p_y^2, xp_x-yp_y\}$ and is equivalent to the linearized scaling ansatz discussed earlier. In general, a quadrupole basis set of order M contains $M(M+1)(2M+7)/6$ elements. Again, expressions useful for numerical calculation of the matrix elements of M, H_0, Σ, and I_c in the quadrupole basis are given in Appendix D.

C. Numerical results

In this section, we present the numerical results obtained by calculating the linear responses to monopole and quadrupole perturbations using the extended basis set approach. We varied λ_d and T/T_F in the range (0,2) at fixed $N = 2200$. We studied the 2D limit $\omega_z = \infty$ as well as a quasi-2D case corresponding to the current experiments with KRb ($\omega_0 = 2\pi \times 36$ Hz, $\omega_z = 2\pi \times 23$ kHz [5]). This choice of parameters yields $\eta \simeq 0.322$ in the quasi-2D case.

For each configuration, we performed the calculations within a fourth-order basis set comprising 35 and 50 basis functions for the monopole and quadrupole cases, respectively, and satisfying all phase-space moments of the CBV equation up to eighth order. The matrix elements of M, H_0, and Σ can be calculated with little computational effort using the expressions provided in Appendixes C and D and the previously obtained equilibrium solutions. The most computationally demanding part is the evaluation of the collision matrix elements. Although a considerable number of them vanish either due to symmetries or conservation laws, a fourth-order basis set still requires calculation of 118 (monopole) and 307 (quadrupole) unique collision matrix elements, each of which is a 5D integral that has to be evaluated for each choice of λ_d, η, and T/T_F. Such a task clearly requires considerably more computational effort compared to the simple scaling ansatz analysis we presented earlier, where only a single collision matrix element had to be dealt with.

We calculated the collision matrix elements using the Monte Carlo integration method with 5×10^8 integration points, yielding a relative statistical error of less than 10^{-3}. We incorporated the dressed quasiparticle dispersions into the collision integral within a local effective mass approximation (see Appendix C 4), which we found to be an excellent approximation in all cases. However, in order to assess the accuracy of this approximation and the consistency of the obtained results, we (1) we performed exact calculation of the collision integrals for a few representative cases using an extrapolation technique (see Appendix E) and (2) checked the satisfaction of conservation laws. We discuss both of these consistency checks later.

For the monopole case, we calculated the dimensionless spectral function $A_{r^2}(\omega)$ defined as

$$A_{r^2}(\omega) \equiv -(2N)^{-\frac{1}{2}}\,\mathrm{Im}[\chi_{r^2}(\omega)], \tag{78}$$

This quantity can be found using Eqs. (53) and (55) by choosing the excitation and observation vectors as $\delta U_\alpha = O_\alpha = \delta_{m\alpha}$, where m is the index that corresponds to the basis function $\phi = r^2$. For the quadrupole case, we calculated the spectral function $A_{x^2-y^2}(\omega)$ defined as

$$A_{x^2-y^2}(\omega) \equiv -(2N)^{-\frac{1}{2}}\,\mathrm{Im}[\chi_{x^2-y^2}(\omega)]. \tag{79}$$

Likewise, this quantity can be evaluated by choosing the excitation and observation vectors as $\delta U_\alpha = O_\alpha = \delta_{q\alpha}$, where q is the index that corresponds to the basis function $\phi = \xi_1 = x^2-y^2$. These spectral functions can be directly measured in the experiments in different ways (Ref. to Sec. VII).

Although the evolution matrix has a large number of eigenmodes, some of which are isolated in the complex plane and some of which may belong to branch lines, only a few of them get excited and contribute to the response. Many of the modes lie inside the null space of H_0, are unphysical, and do not get excited (see the discussion at the end of Sec. V A). In all cases, we found that the spectral functions can be reproduced accurately by a fit function with two simple poles in the lower half plane,

$$A_{\mathrm{fit}}(\omega) = \mathrm{Im}\left[\frac{\mathcal{A}}{\omega-\Omega-i\Gamma} - \frac{\mathcal{A}^*}{\omega+\Omega-i\Gamma} + \frac{i\mathcal{B}}{\omega-i\Gamma'}\right], \tag{80}$$

corresponding to damped oscillations with a frequency and damping rate of Ω and Γ, respectively, and a possibly overdamped component with a decay rate of Γ'. The overdamped component is only present in the quadrupole response. The above model extracts the most important features of the numerically obtained spectral functions and also allows us to present the obtained results in a concise way.

Although we kept up to 8 moments (and in some cases, up to 12 moments) of the CBV equation, we found the inclusion of sixth-order moments (and above) to result in relative refinements to the frequency of the first and second excited modes, which are smaller than 10^{-3} and 10^{-2}, respectively, in all cases.

1. Monopole oscillations

As mentioned earlier in Sec. V A, without self-energy corrections, the CBV equation for harmonically trapped gases admits an exact solution corresponding to a scaling velocity field $\mathbf{v}\sim\mathbf{r}$, which has a fixed oscillation frequency of $2\omega_0$ with no damping, independent of the interaction strength and temperature. This is due to fact that the Boltzmann equation admits a rigorously closed set of equations for the phase-space averages of r^2, p^2 and $\mathbf{r}\cdot\mathbf{p}$, all of which are unaffected by collisions due to conservation laws. Taking self-energy corrections into account, the quasiparticle dispersions no longer remain quadratic and one finds that this simple chain of moment equations cannot be closed anymore. In particular, contributions from higher-order moments, many of which are strongly influenced by the collisions, become important. Therefore, we expect the monopole oscillations to be damped to a certain degree.

Figure 6 shows the frequency and damping of the monopole oscillations extracted from the numerically obtained spectral functions. The colored and grayscale (top and bottom,

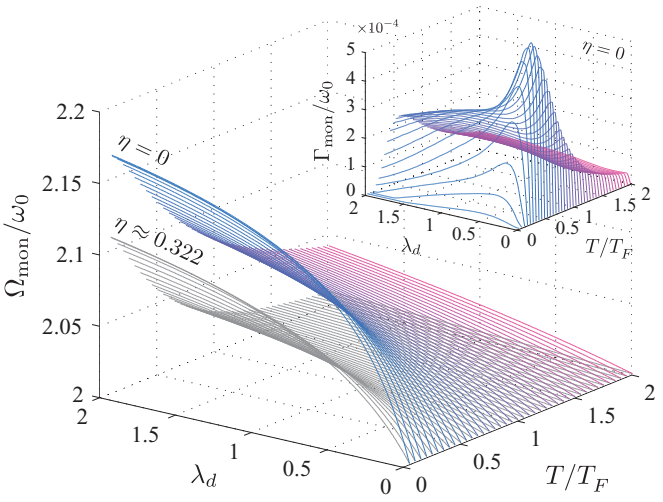

FIG. 6. (Color online) The oscillation frequency and the damping (inset) of the monopole excitations extracted from the numerically obtained spectral functions using a fourth-order basis set (including self-energy corrections). The colored and grayscale (upper and lower) graphs correspond to an ideal 2D system ($\eta = 0$) and a quasi-2D system ($\eta \simeq 0.322$), respectively. Blue and red line colors correspond to low and high temperatures, respectively. In all cases, $N = 2200$. The inset plot shows the damping rate in the 2D case ($\eta = 0$).

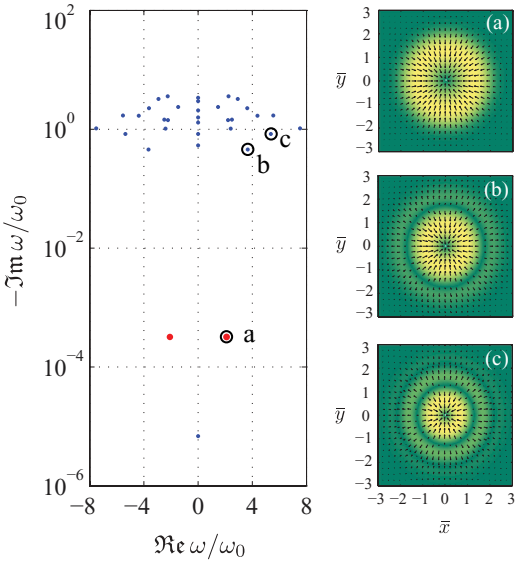

FIG. 7. (Color online) (left) A typical picture of the poles of the evolution matrix ($T/T_F = 0.45$, $\lambda_d = 2$, $N = 2200$, and $\eta = 0$). (Right) The mass currents associated with the indicated poles. Yellow (bright) and green (dark) background colors indicate large and small current magnitudes, respectively. The three indicated poles (a), (b), and (c) have the largest residues in the monopole response function and are also the lowest-lying modes that survive in the collision-dominated regime.

respectively) plots correspond to the 2D limit ($\eta = 0$) and a quasi-2D sample ($\eta \simeq 0.322$). The repulsive dipole-dipole interactions clearly result in a significant increase in the oscillation frequency. Also, as one expects, finite transverse confinement leads to a weaker effective repulsive effective interaction and, thus, a smaller increase in the frequency of collective modes.

Figure 7 shows a typical plot of the poles of the evolution matrix as well as the mass currents associated with the three lowest-lying modes that get excited by the monopole perturbation. The lowest-lying mode (indicated by "a" and having a nodeless mass current) makes the most contribution. In fact, the relative spectral weight of all other modes are generally found to be less than $\sim 10^{-3}$ in all cases. We label the monopole modes according to the number of nodes in their mass current; that is, (a), (b), and (c) correspond to $n = 0$, 1, and 2, respectively.

The most intriguing finding is that the nodeless mode exhibits a negligible damping in all of the studied cases despite the presence of remarkably large self-energy corrections ($\Gamma_{\rm mon} < 10^{-3}\omega_0$; see the inset plot of Fig. 6). This is, however, not the case for the higher-order modes. Figure 8 shows the evolution of $n = 0$ and $n = 1$ modes upon increasing T at fixed λ_d for a 2D [panels (a) and (b)] and a quasi-2D system [panels (c) and (d)]. The behavior of the $n = 0$ mode is similar in 2D and quasi-2D: The rise in temperature reduces the self-energy effects and the frequency approaches its noninteracting value of $2\omega_0$. The damping remains small $\sim 10^{-4}\omega_0$ and exhibits a peak around $T \sim T_F$. While the mode eventually becomes CL in quasi-2D (for $T \gg \hbar\omega_z$), on the contrary, it reaches a plateau in 2D. The difference between 2D and quasi-2D systems is more striking for $n = 1$ and higher-order modes: Upon increasing T, while the frequency of oscillations monotonically decreases in 2D until it reaches

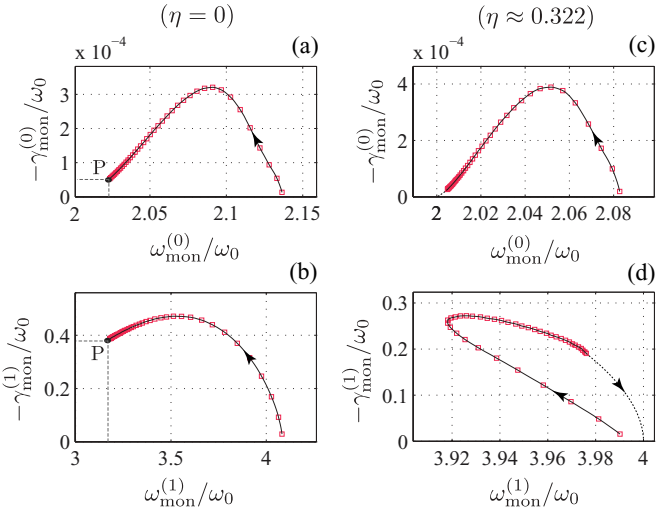

FIG. 8. (Color online) The evolution of the two lowest-lying monopole modes upon increasing T at fixed $\lambda_d = 1$ and $N = 2200$. The temperature is uniformly increased from $T/T_F = 0.05$ to $T/T_F = 2$ with 0.05 increments. $\omega^{(n)}$ and $\gamma^{(n)}$ denote the real and imaginary parts of the complex eigenvalue, respectively. The arrows indicates the direction of increasing T. Panels (a) and (b) correspond to the $n = 0$ and $n = 1$ modes, respectively, for a 2D system ($\eta = 0$). Panels (c) and (d) show the same quantities for a sample quasi-2D system ($\eta \approx 0.322$). While the 2D system reaches a plateau for $T \gg T_F$ (indicated by P), the quasi-2D system eventually becomes CL; that is, $\gamma^{(i)}_{\rm mon} \to 0$, $\omega^{(n)}_{\rm mon} \to 2(n+1)\,\omega_0$. The dashed lines show this expected behavior qualitatively.

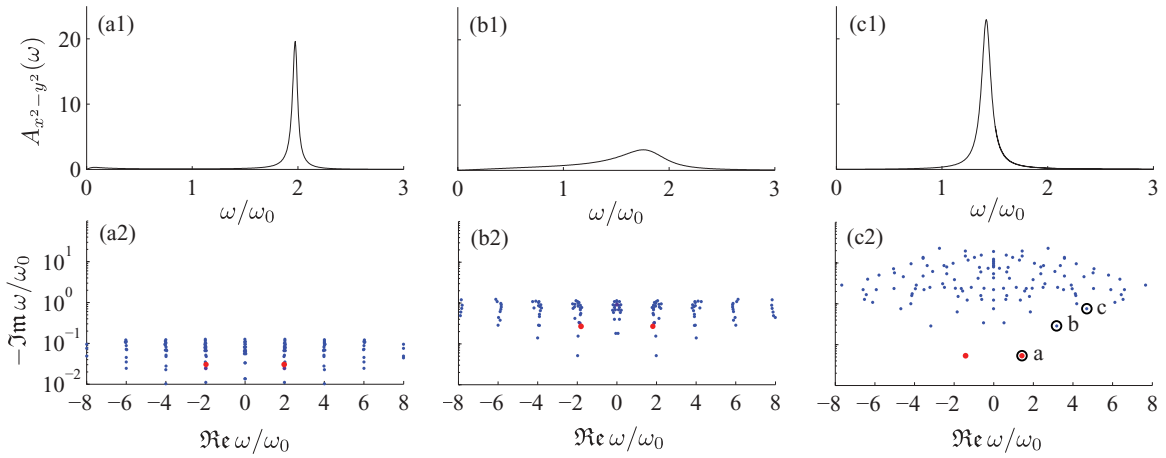

FIG. 9. (Color online) Evolution of the quadrupole oscillations from CL to HD regime upon increasing the interaction strength (left to right). In all cases, $T/T_F = 0.45$ and $\eta = 0$ ($\omega_z = \infty$). The top row shows the quadrupole spectral function and the bottom row shows the locations of the poles of the evolution matrix on the complex plane. The pole shown as red is the pole that makes the dominant contribution to the response. (a1) and (a2) $\lambda_d = 0.1$; (b1) and (b2) $\lambda_d = 0.4$; (c1) and (c2) $\lambda_d = 2$. See Fig. 10 for a plot of the mass currents associated with the encircled poles. Refer to Sec. VII for a discussion on the experimental methods of measuring the spectral functions.

the plateau, it has a nonmonotonic behavior in quasi-2D. Initially, it decreases due to enhanced collisions and reduced self-energy effects. Once $T \sim \hbar\omega_z$, the collision rate starts to decrease and the mode eventually becomes CL. A qualitative account of this behavior was given in Sec. V B. Finally, we note that the character of the plateau in 2D is determined by λ_d and N, and the modes in the plateau may lie anywhere in the CL-HD spectrum.

In summary, we find that the monopole response is governed predominantly by the lowest-lying (nodeless) mode, with the higher-order modes capturing a relative spectral weight of less than 10^{-3}. The collisional effects play a little role in defining the character of this dominant mode. In contrast, the higher-order modes are found to be significantly affected by collisions. They undergo a transition from the CL to the HD regime.

2. *Quadrupole oscillations*

In the previous section, we found that the nodeless monopole mode is essentially immune to collisions. This is not the case for the nodeless quadrupole mode. The scaling ansatz analysis presented earlier already shows that this mode is, in fact, strongly affected by collisions.

Similar to the monopole case, we find that quadrupole perturbations of the trap potential primarily excite the lowest-lying quadrupole mode and the relative spectral weight of higher-order modes are generally less than 10^{-3}. In this case, however, we find a small but significant contribution from a few overdamped modes, especially in the crossover regime. This is in agreement with the scaling ansatz analysis.

A typical scenario for the quadrupole response is shown in Fig. 9. The top and bottom rows show the quadrupole spectral function and the location of the poles on the complex frequency plane, respectively. For weak interactions [$\lambda_d \ll 1$, Figs. 9(a1) and 9(a2)], the spectral function is sharply peaked around $2\omega_0$ and the poles of the evolution matrix lie very close to the real axis about their CL frequencies. Upon increasing the interactions, the poles spread to the lower half complex frequency plane, indicating entrance to the dissipative CL-HD crossover regime. The spectral function is significantly broadened [see Fig. 9(b1)] in this regime. For stronger interactions, the local equilibrium picture starts to emerge, indicated by a reduction in damping. Figure 9(c2) clearly shows a sharply peaked spectral function near $\sqrt{2}\omega_0$ in the strongly interacting regime. This is exactly the universal frequency of the HD quadrupole surface mode discussed earlier.

Figure 10 shows the mass currents associated to the three lowest-lying modes marked in Fig. 9(c2). The axially averaged mass currents have $n = 0$, 1, and 2 nodes respectively. Figure 11 shows the evolution of the first two upon increasing the temperature for a 2D and a quasi-2D case. Both modes are strongly influenced by collisions and their qualitative behavior is similar to the $n = 1$ monopole mode discussed in the previous section. While these modes eventually become CL in quasi-2D for $T \gg \hbar\omega_z$, they reach a plateau for $T \gg T_F$ in 2D [marked with P in (a) and (b)].

Figures 12 and 13 show the frequency and damping rate of the quadrupole oscillations obtained from the fit to the quadrupole spectral function, in 2D and quasi-2D, respectively.

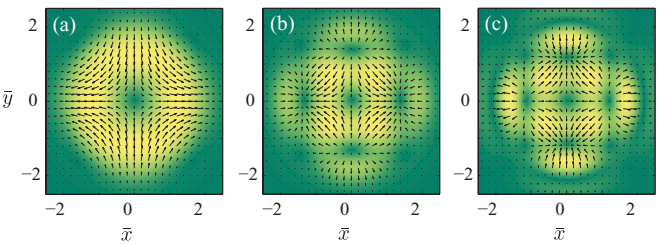

FIG. 10. (Color online) The mass current associated to the three modes marked in Fig. 9(c2). Yellow (bright) and green (dark) shades indicate large and small current magnitudes, respectively. (a) The lowest lying mode, known as the surface mode, characterized by the velocity field $\mathbf{v} \sim x\mathbf{e}_x - y\mathbf{e}_y$; (b),(c) the next two modes. The nodal structure of the mass current is clearly noticeable.

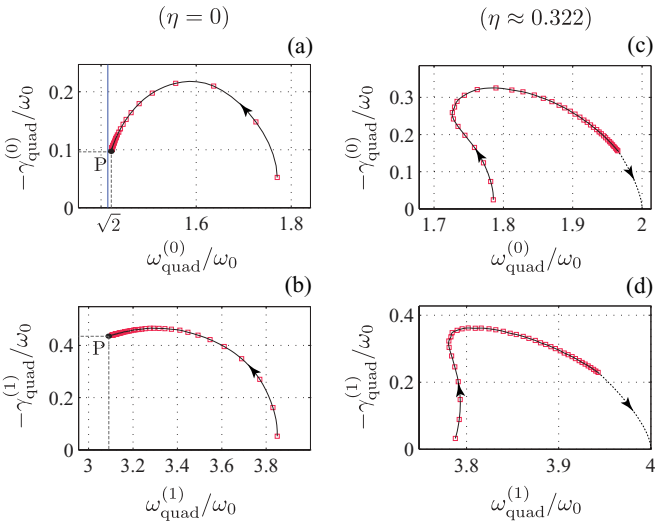

FIG. 11. (Color online) The evolution of the two lowest-lying quadrupole modes upon increasing T for fixed $\lambda_d = 1$ and $N = 2200$. See the caption of Fig. 8 for the description of various panels. The blue line in (a) denotes $\sqrt{2}\omega_0$, the frequency of quadrupole surface mode.

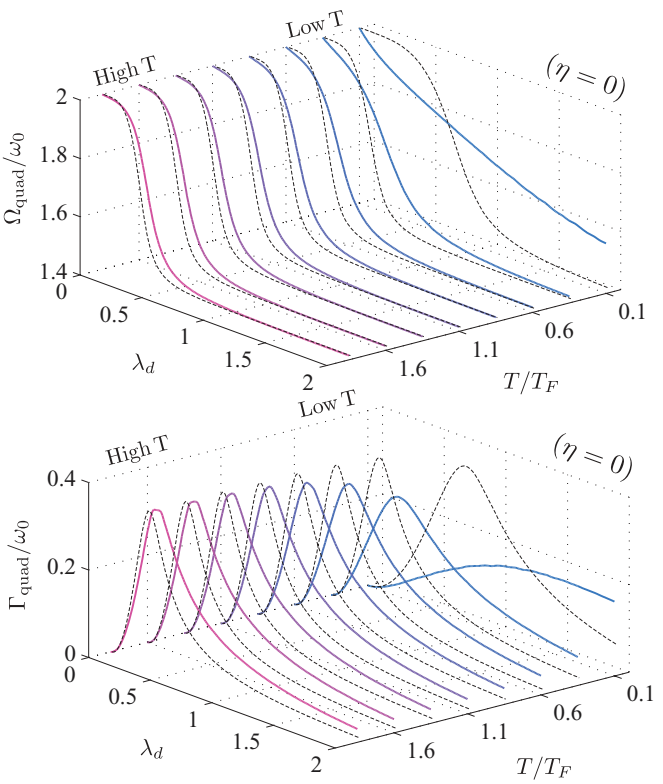

FIG. 12. (Color online) Frequency and damping (top and bottom graphs, respectively) of quadrupole oscillations in a 2D system ($\eta = 0$) with $N = 2200$ particles. The solid colored lines are the numerical results obtained using a fourth-order basis set, including self-energy corrections. The red and blue line colors denote high and low temperatures, respectively. The dashed black lines correspond to the analytic scaling ansatz analysis presented earlier (Sec. V B).

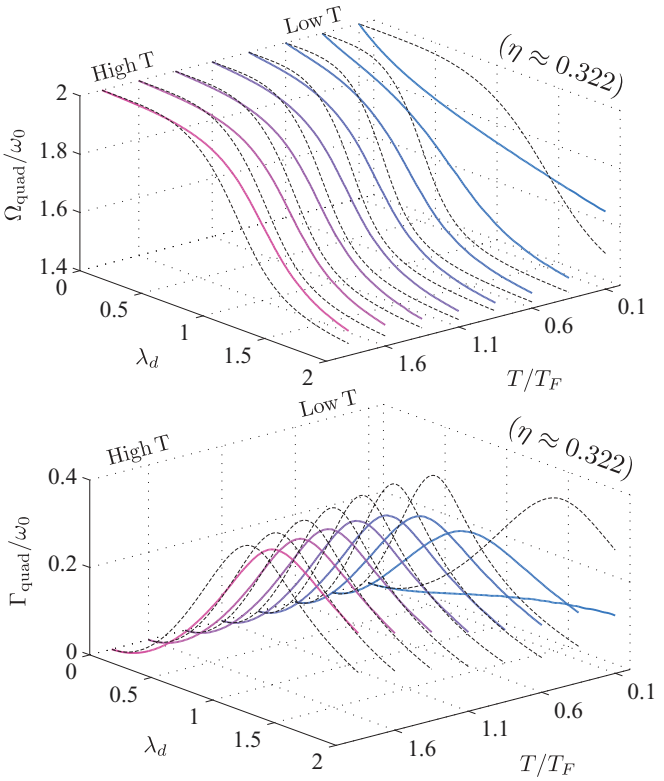

FIG. 13. (Color online) Frequency and damping of quadrupole oscillations for a quasi-2D system corresponding to $\eta \simeq 0.322$ (refer to the caption of Fig. 12 for details).

The result from the previous scaling ansatz analysis without self-energy corrections is also shown as dashed black lines for reference. Since the quadrupole spectral function is virtually exhausted by the nodeless mode, these plots essentially show the interaction and temperature dependence of the nodeless mode.

The refinements arising from inclusion of both self-energy corrections and higher-order moments are significant. In the low-temperature regime, self-energy corrections are dominant and yield a $\propto\lambda_d$ shift of the frequencies (see the rightmost plot in the top panel of Fig. 12). The collisional corrections are only $\propto\lambda_d^4$ in the weakly interacting regime [see Eq. (72) and note that $\nu_c \propto \lambda_d^2$]. The corrections resulting from the inclusion of higher-order moments can also be seen in the high-temperature curves appearing in the same figure. For $T > T_F$, self-energy corrections become negligible and the refinement is predominantly due to inclusion of higher-order moments.

In summary, we find that all quadrupole modes are strongly influenced by collisions and exhibit the transition from the CL to the HD regime. There is a notably large mean-field shift in the oscillation frequency at low temperatures. Similar to the monopole case, the quadrupole spectral function is essentially exhausted by the lowest-lying (nodeless) mode, with a small contribution from overdamped modes in the crossover regime. Upon increasing the temperature, the frequency and damping of all modes reach a plateau for a strictly 2D system. A qualitative account of this behavior was given in Sec. V B. In a quasi-2D system, however, the CL regime appears again for $T \gtrsim \hbar\omega_z$.

VII. EXPERIMENTAL OUTLOOK

The collective modes can be probed experimentally in various ways. As described earlier, one common method is to perturb the trap potential with a short pulse and monitor the evolution of the cloud using either *in situ* or absorption imaging techniques (for example, see Ref. [9]). The relevant observables are the radius and anisotropy of the cloud in case of monopole and quadrupole perturbations, respectively. The frequency and damping of the collective modes are found by fitting the measured time evolution of the observable $O_{\rm exp}(t)$ to a function of the form $O_{\rm fit}(t) = Ae^{-\gamma t}\sin(\omega t+\phi_0) + Be^{-\gamma_{\rm OD}t}$, where ω is the frequency of oscillations, and γ and $\gamma_{\rm OD}$ are damping rate of the oscillatory and overdamped components, respectively. If required, the spectral function can be subsequently found by taking a Fourier transform of the measured impulse response signal $O_{\rm exp}(t)$. Another approach which may yield more accurate results is the direct measurement of spectral functions via trap modulation spectroscopy. In this method, one introduces a low-amplitude periodic modulation at a fixed frequency Ω to the trap potential for a duration $\tau \gg \omega_0^{-1}, \Omega^{-1}$ and measures the absorbed energy. For a finite trap modulation pulse such as $\delta U \sim e^{-|t|/\tau}\cos(\Omega t)\, v(\mathbf{r})$, a simple linear response analysis yields [43]

$$\Delta E_{\rm abs} \sim -\tau\, \Omega\, {\rm Im}[\chi_{v(\mathbf{r})}(\Omega + i/\tau)], \tag{81}$$

where $\Delta E_{\rm abs}$ is the absorbed energy, $v(\mathbf{r})$ is the shape of the trap perturbation (i.e., x^2+y^2 and x^2-y^2 for monopole and quadrupole modes respectively), and $\chi_{v(\mathbf{r})}$ is the retarded response function of $v(\mathbf{r})$. Equation (81) implies that the absorbed energy in a modulation experiment provides a direct measurement of the spectral function. The absorbed energy can be measured in various ways. One method is to let the system rethermalize after the modulation pulse, followed by mapping it to a noninteracting system by switching off the interactions adiabatically and finally measuring the temperature rise of the noninteracting gas through a time-of-flight expansion experiment. The location of the peak in the measured spectral function and its width yield the frequency and damping of the collective mode. According to the results presented in the previous section, quadratic perturbations in the trap potential predominantly excite the lowest-lying mode. If required, the spectral weight of higher-order modes can be increased using quartic perturbations, for example, $(x^2+y^2)^2$ and x^4-y^4 for monopole and quadrupole symmetries, respectively.

At the time this paper was written, the dipolar interaction strengths in the experiments were not strong enough to possibly drive the system to the HD regime. In the experiments with fermionic ^{40}K-^{87}Rb at JILA [5], the transverse and in-plane trap frequencies are $\omega_z = (2\pi)\times 23$ kHz and $\omega_0 = (2\pi)\times 36$ Hz, respectively. The central layer has 2200 molecules, the temperature is $T = 500$ nK and the dipole moment is $D = 0.158$ debye, using which we find $T/T_F \approx 4.36$, $\eta \approx 0.322$, and $\lambda_d \approx 0.252$. The dipolar temperature is $T_{\rm dip} \sim 1.8\ \mu$K and $T_F/T_{\rm dip} \approx 6.4\times 10^{-2}$. Therefore, the near-threshold scattering condition can be satisfied well for quantum degenerate temperatures. However, the lowest achievable temperature in the current experiments is well above quantum degeneracy and $T/T_{\rm dip} \approx 0.28$. The scattering energies lie in the crossover between the threshold and semiclassical energies and we estimate the Born approximation to overestimate the cross section by a factor of 3 using the results of Ref. [28]. Since the temperature is high, mean-field corrections are small and the change in the monopole oscillation frequency is negligible. For quadrupole oscillations, we obtain $\Omega_{\rm quad} \approx 1.9990\,\omega_0$ and $\Gamma_{\rm quad} \approx 0.007\,\omega_0 = 1.7$ Hz. Including corrections to the Born approximation, we estimate $\Gamma_{\rm quad} \approx 0.6$ Hz which might be difficult to observe due to the presence of a two-body loss rate of ~ 4 Hz Ref. [5]. We remark that the collision rates can be dramatically increased by making the transverse confinement stronger. For example, in the strictly 2D limit $\omega_z \to \infty$, we get $\Omega^{\rm 2D}_{\rm quad} \approx 1.8\,\omega_0$ and $\Gamma^{\rm 2D}_{\rm quad} \approx 0.3\,\omega_0 \approx 71$ Hz at the same temperature and phase-space density.

The experiment with ^{161}Dy [8] at Stanford is another promising candidate to observe the predictions of this paper. With $N = 6000$ atoms at a temperature $T/T_F = 0.21$ and a large magnetic dipole moment of $10\mu_B$, one is able to study both quantum degenerate and thermal regimes. Once the atoms are loaded into an optical lattice, we believe it will be possible to trap at least $N = 2000$ atoms at the Fermi temperature in the central pancake, with $\omega_z = (2\pi)\times 20$ kHz and $\omega_0 = (2\pi)\times 100$ Hz. For this configuration, we find $T_F/T_{\rm dip} \approx 0.04$, $\lambda_d \approx 0.21$, and $\eta \approx 0.56$. The near-threshold condition is satisfied well and we reliably obtain $\Omega_{\rm quad} \approx 1.992\,\omega_0$ and $\Gamma_{\rm quad} \approx 0.0085\,\omega_0 \approx 5.3$ Hz. That damping is expected to be easily observable due to the long-time stability of the gas. The mean-field shifts of the frequencies may also be observed at lower temperatures. With $N = 1000$ atoms in the central pancake and at $T/T_F = 0.2$ and the same trap frequencies, we obtain $\Omega_{\rm quad} \approx 1.95\,\omega_0$ and $\Gamma_{\rm quad} \approx 0.0065\,\omega_0 \approx 4.8$ Hz, and $\Omega_{\rm mon} - 2\omega_0 = 0.015\,\omega_0 \approx 9.3$ Hz, all of which are expected to be observable. Another intriguing possibility is the observation of the predicted plateau of the collision rate, which is also a direct consequence of universal near-threshold dipolar scatterings. This can be simply done by heating the gas and probing the collective modes at temperatures above T_F.

VIII. DISCUSSIONS

Most of the relevant discussions were already given in the main text. Here, we give a brief summary of the main results along with several complementary comments.

We started our analysis by investigating the equilibrium state of quasi-2D dipolar fermions in isotropic traps. In order to study the collective modes of the system, we solved the collisional Boltzmann-Vlasov equation for small perturbations of the trap potential with monopole and quadrupole symmetries. The self-energy corrections to quasiparticle dispersions and collisions were taken into account via the self-consistent HF and Born approximations, respectively. The validity of these approximations were assessed at the end of Sec. II C. In particular, the usage of Born approximation restricts the validity domain of our results to near-threshold scattering energies [see Eq. (25)]. We confined our attention to the regime where $T_F \ll T_{\rm dip}$, so that the scatterings remain in the near-threshold regime even in the thermal regime $T \gg T_F$. We showed that this condition is satisfied well in the current experiments. We emphasize that once the conditions for the applicability of our approximations are met, the formalism of collisional

Boltzmann-Vlasov equation is universally applicable to both CL and collision-dominated (HD) regimes, as well as the crossover between the two.

We carried out the analysis of collective modes in two stages. As a first approximation, we studied the problem in the Boltzmann limit by only keeping the collisional effects and using bare dispersions. We calculated the response functions using the simple picture of scaling ansatz. This analysis implied the generic result that monopole oscillations occur at a fixed frequency of $2\omega_0$, are undamped, and are independent of temperature and interaction strength. In case of quadrupole oscillations, however, we found a transition from the CL limit to the HD limit. We calculated the quadrupole collision rate, ν_c, for various temperatures and transverse trap frequencies. We found that in the 2D limit ($\eta = 0$), ν_c is a monotonically increasing function of temperature and reaches a plateau for large T/T_F. This plateau persists up to $T \simeq T_{\rm dip}$, beyond which the scattering energies enter the semiclassical regime and the cross section starts to decrease upon increasing the temperature further. The existence of this plateau, which is a unique feature of dipolar scatterings implies that (1) the character of trap excitations of a polarized 2D dipolar gas becomes essentially temperature independent in the regime $T_F \lesssim T \lesssim T_{\rm dip}$ and (2) collisional effects persists in the thermal regime despite the fact that gas becomes very dilute. This behavior differentiates 2D dipolar fermionic gases from s-wave fermions where rarefaction of the gas at high temperatures carries the system back to the CL regime for $T \gtrsim T_F$. Also, the temperature window for collisional behavior is universal for s-wave fermions and is not amenable to tuning, whereas for quasi-2D dipolar fermions, one can expand this window by (1) making the transverse confinement stronger to approach the 2D limit and (2) either increasing $T_{\rm dip}$ by using weaker dipoles or decreasing T_F by decreasing the density.

The existence of the plateau is guaranteed as long as the scale separation $T_F \ll T_{\rm dip}$ is met. Combining Eqs. (25) and (67), one can find the condition for the plateau to lie in the collision-dominated (HD) regime as well:

$$N^{\frac{1}{4}} \ll \frac{a_0}{a_d} \ll N^{\frac{1}{2}} \quad \text{(HD plateau)}. \tag{82}$$

The left- and right-hand sides of this inequality are equivalent to $T_F \ll T_{\rm dip}$ and $N(a_d/a_0)^2 \gg 1$, respectively, where the latter condition implies $\nu_c \gg 1$. The above inequality may be used as a simple experimental guideline to observe HD behavior with dipolar fermions.

In the second stage of calculations, we extended the analysis by (1) including self-energy corrections and (2) going beyond the scaling ansatz by satisfying higher moments of the CBV equation. Chiacchiera *et al.* [35] and Pantel *et al.* [41] have carried out a similar extended moments analysis of the Boltzmann equation for s-wave fermions and have shown that corrections of this type significantly improve the matching between the theory and the experiments.

We evaluated all of the matrix elements of the CBV equation numerically exactly with the exception of the collision integral matrix elements where we incorporated the dressed quasiparticle dispersions via a local effective mass approximation (LEMA) for practical reasons. Nevertheless, we found this scheme to be an excellent approximation. We show later in this section that the conservation laws are satisfied well. Moreover, we evaluated the exact collision matrix elements in a few cases using an extrapolation technique (albeit at the costs of a significantly increased computation time; see Appendix E) and found the corrections beyond LEMA to be negligible indeed.

The extension of the scaling ansatz analysis allowed us to (1) study the effects of self-energy corrections on the frequency and damping of various modes, (2) investigate the higher-order (nodal) monopole and quadrupole modes which are beyond the scope of the scaling ansatz, and (3) study the speculated damping of the nodeless monopole mode, which is a direct consequence of self-energy corrections. We found that despite the fact that inclusion of higher-order moments results in the appearance of numerous new normal modes, the responses to the monopole and quadrupole perturbations ($\sim r^2$ and $x^2 - y^2$, respectively) are predominantly governed by the lowest-lying (nodeless) mode. We remark that the frequency and damping of the mode, however, is significantly modified by both self-energy corrections and inclusion of higher-order moments.

We argued that the self-energy corrections are expected to result in the damping of the nodeless monopole mode, a feature which is absent in the simple Boltzmann equation. We found that although this expectation is met, the damping remains very small ($<10^{-3}\omega_0$), even in the strongly interacting regime. The frequency of oscillations, however, is significantly increased from its noninteracting value of $2\omega_0$. This mean-field frequency shift was found to be most significant at low temperatures where self-energy effects are large.

By investigating the velocity field of nodeless monopole mode, we found that it retains its scaling character to a good approximation (i.e., $\mathbf{v} \sim \mathbf{r}$), as well as its isothermal character. It is known from the HD theory of nonideal fluids that for a true isotropic and isothermal scaling flow, no dissipation results from shear viscosity or thermal conduction and the only source of dissipation is the bulk viscosity (for instance, see Ref. [42], Sec. 49). In this situation, one finds $dS/dt = \int d^2\mathbf{r}\, n_0^{-1} T^{-1} \zeta (\boldsymbol{\nabla} \cdot \mathbf{v})^2$, where S is the total entropy and ζ is the bulk viscosity. Note that the dissipation rate is second order in $\mathbf{v}$ and is therefore small.

At this point, we cannot rule out the possibility that a more accurate description of the strongly correlated regime would change this finding. In particular, going beyond the quasiparticle ansatz in the kinetic equation and taking the collisional broadening of the single-particle spectrum into account may yield a larger damping of the nodeless monopole mode. We will investigate this possibility in the future works.

The analysis of higher-order monopole modes ($n \geqslant 1$) and all quadrupole modes yields the same qualitative picture that the scaling ansatz analysis of the nodeless quadrupole mode provides, that is, existence of a plateau in 2D upon increasing the temperature and reappearance of the CL regime in quasi-2D. We find, however, significant quantitative corrections. At low temperatures, self-energy corrections result in a shift of the frequencies proportional to λ_d. We also found that the scaling ansatz overestimates the collision rates in general. This defect is mostly noticeable in the high-temperature regime where the gas is extended in the trap and higher-order moments are required to accurately account for the density variations.

We included up to 8 moments in the extended analysis (and up to 12 moments in pilot studies). We generally found

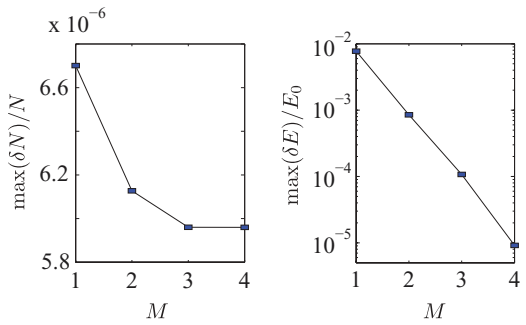

FIG. 14. Maximum relative deviations of the particle number (left) and energy (right) for monopole oscillations in a sample configuration ($T/T_F = 0.1$, $\lambda_d = 0.5$, $\eta = 0$ and $N = 2200$). M is the truncation order of the basis set.

that the most important corrections to the scaling ansatz stems from the fourth-order moments, beyond which the corrections become increasingly smaller. In practice, a second-order basis set is sufficient to obtain the frequencies of the nodeless modes within a 0.1% tolerance of the exact solution. The accurate description of higher-order modes naturally require inclusion of higher-order moments.

Finally, we investigate the satisfaction of conservation laws as a consistency check for our numerical calculations. The CBV equation conserves the particle number, momentum, and energy, both in the differential form and the integral form (see Appendix A). The quadrupole oscillations trivially satisfy these conservation laws due to the axial symmetry of the equilibrium state. This is not trivial for monopole oscillations as they have same symmetry as the equilibrium state. Figure 14 shows the maximum relative deviations of the particle number and energy in monopole oscillations as a function of moment satisfaction order for a sample case. We find that the particle number is conserved within a relative error of $\sim 10^{-6}$ even in a first-order basis set (this is because one of the moment equations is in fact a statement of mass conservation). On the other hand, we find that conservation of energy improves substantially upon extending the basis set. For the fourth-order basis set, the relative error in the conservation of energy is $\sim 10^{-5}$.

Some of the possible extensions of this work are (1) going beyond the Born approximation and including multiple scatterings in order to rigorously extend this study to semiclassical scattering energies ($T > T_{\rm dip}$), (2) going beyond the quasiparticle approximation and taking into account the collisional broadening of the single-particle spectrum toward quantitatively reliable predictions in the strongly interacting regime, and (3) inclusion of higher transverse subbands to account for $T \gtrsim \hbar\omega_z$ in quasi-2D systems.

ACKNOWLEDGMENTS

The computations in this paper were run on the Odyssey cluster supported by the FAS Science Division Research Computing Group at Harvard University. M. Babadi would like to thank K. Baumann for useful discussions. The authors acknowledge the support from Harvard-MIT CUA, NSF Grant No. DMR-07-05472, DARPA OLE program, AFOSR Quantum Simulation MURI, AFOSR MURI on Ultracold Molecules, and the ARO-MURI on Atomtronics.

APPENDIX A: CONSERVATION LAWS OF THE LINEARIZED COLLISIONAL BOLTZMANN-VLASOV EQUATION

The CBV equation admits local conservation laws for mass density, mass current, and energy, which can be simply established by multiplying the sides of CBV equation by 1, $\mathbf{p}$, and energy density $\mathcal{E}$, respectively, and integrating over $\mathbf{p}$ [20]. Here, $\mathcal{E}$ is the energy density. The collision integrals vanish identically in all three cases due to the existence of the same conservation laws in the level of two-body scatterings. We state these conservation laws in their integral form here and utilize them later as a consistency check for our numerical calculations. The conservation of mass (or equivalently, particle number) is

$$\frac{d}{dt}\int d\Gamma\, n(\mathbf{p};\mathbf{r},t) = 0. \tag{A1}$$

The linearized equation using the parametrization given by Eq. (40) yields

$$\frac{d}{dt}\int d\Gamma\, \Delta_0\Phi(\mathbf{p};\mathbf{r},t) = 0. \tag{A2}$$

In the same parametrization, the conservation of momentum reads as

$$\frac{d}{dt}\int d\Gamma\, \mathbf{p}\, \Delta_0\Phi(\mathbf{p};\mathbf{r},t) = 0. \tag{A3}$$

The energy density is given by $\mathcal{E}_{\rm HF} = p^2/(2m) + m\omega_0^2 r^2/2 + \Sigma^+[n]/2$ in the HF approximation, using which we get the following linearized form of conservation of energy:

$$\frac{d}{dt}\int d\Gamma(\delta\mathcal{E}\, n_0 + \mathcal{E}_0\Delta_0\Phi(\mathbf{p};\mathbf{r},t)) = 0, \tag{A4}$$

where $\mathcal{E}_0 \equiv \mathcal{H}_0$ is the equilibrium energy density and $\delta\mathcal{E} = \Sigma^+[\delta n]/2 = \Sigma^+[\Delta_0\Phi]/2$. Using the properties of HF self-energy functional, it is easy to show $\int d\Gamma\, \delta\mathcal{E}\, n_0 = (1/2)\int d\Gamma\, \Sigma^+[\Delta_0\Phi]\, n_0 \equiv (1/2)\int d\Gamma\, \Sigma^+[n_0]\, \Delta_0\Phi$, using which the two terms in Eq. (A4) can be combined to yield

$$\frac{d}{dt}\int d\Gamma\, \mathcal{H}_0\Delta_0\Phi(\mathbf{p};\mathbf{r},t) = 0. \tag{A5}$$

APPENDIX B: ASYMPTOTIC ANALYSIS OF $Q(\bar{T},\eta = 0)$

In the 2D limit ($\eta = 0$), the asymptotic behavior of $Q(\bar{T},\eta)$ can be studied analytically. Setting $\eta = 0$, the Erfcx functions appearing in the collision integral [see Eq. (66)] evaluate to unity and the expression in the brackets in the second line simply becomes $[\chi_1 - \chi_2]^2 = \sin^2\xi\, \sin^2\nu\, [1 - |\sin(\phi - \phi')|]$. This results in significant simplifications.

1. Low-temperature expansion

In the low-temperature regime, $\bar{\mu}/\bar{T} \to \infty$, we may use the following identity:

$$\lim_{\bar{\mu}/\bar{T}\to\infty} (\bar{\mu}/\bar{T})^{-3} \int_0^\infty \rho^5\, d\rho \left[\frac{1}{\cosh(\rho-\bar{\mu}/\bar{T})+\cosh(b_1\rho)} \times \frac{1}{\cosh(\rho-\bar{\mu}/\bar{T})+\cosh(b_2\rho)}\right] = \frac{4\pi^2}{3}\,\delta(b_1)\,\delta(b_2). \tag{B1}$$

The above identity can be established by observing that for large $\bar{\beta}\bar{\mu}$ the integrand is exponentially small unless $\rho \sim \bar{\beta}\bar{\mu}$ and $b_1, b_2 \sim (\bar{\beta}\bar{\mu})^{-1}$. In the limit $\bar{\beta}\bar{\mu} \to \infty$, the right-hand side becomes proportional to $\delta(b_1)\,\delta(b_2)$. The proportionality constant can be found by integrating the left-hand side over b_1 and b_2, which gives the $4\pi^2/3$ prefactor. Identifying b_1 and b_2 as $\sin^2\xi\,\sin 2\nu\,\cos\phi$ and $\sin^2\xi\,\sin 2\nu\,\cos\phi'$, respectively, we can carry out the ξ and ν integrations using the δ functions and we finally get

$$Q(\bar{T}\to 0,\eta=0) \approx C\,\frac{(\bar{\mu}/\bar{T})^3}{\langle\!\langle \bar{p}^4\rangle\!\rangle}, \tag{B2}$$

where C is given by

$$C = \frac{32}{9}\int_0^{2\pi} d\phi \int_0^{2\pi} d\phi' \frac{[1-|\sin(\phi-\phi')|]\,\sin(\phi-\phi')^2}{\cos^2\phi+\cos^2\phi'} \tag{B3}$$

and is equal to 19.176 999 to six decimal places. $\langle\!\langle \bar{p}^4\rangle\!\rangle$ can be found analytically with little effort and we get

$$\langle\!\langle \bar{p}^4\rangle\!\rangle = -8\bar{T}^3\,\mathrm{Li}_3(-e^{\bar{\mu}/\bar{T}}). \tag{B4}$$

Using the asymptotic expansion of $\mathrm{Li}_3(-x)$ for large x and the low-temperature expansion of $\bar{\mu}$ mentioned after Eq. (34), the following low-temperature expansion follows:

$$-\mathrm{Li}_3(-e^{\bar{\mu}/\bar{T}}) = 1/(6\bar{T}^3)+\pi^2/(12\bar{T})+O(\bar{T}). \tag{B5}$$

Combining the last four equations, we finally get

$$Q(\bar{T}\to 0,\eta=0) \approx \tfrac{2}{3}\,C\,\bar{T}^2 \approx 12.784\,666\,\bar{T}^2 \tag{B6}$$

to leading order. This asymptotic limit is shown in Fig. 5(e) as a blue dashed line and agrees well with the numerical result.

2. High-temperature expansion

The analysis of the classical limit ($\bar{\beta}\bar{\mu} \to 0$) is simpler. First, we rewrite the hyperbolic functions in the denominator as $\cosh(\rho-\ln z) \equiv e^\rho/(2z)+(z/2)e^{-\rho}$. Here, $z \equiv \exp(\bar{\mu}/\bar{T})$ is the fugacity and goes to zero in the high-temperature limit. Thus, $\cosh(\rho-\ln z) \approx e^\rho/(2z)$ to leading order. The denominator of Eq. (66) is dominated by the first cosh term. Neglecting the second cosh terms, the integrations become elementary and we get

$$Q(\bar{T}\to 0,\eta=0) \approx \frac{8(8-3\pi)z^2\bar{T}^5}{\langle\!\langle \bar{p}^4\rangle\!\rangle}. \tag{B7}$$

The fugacity in the classical limit can be found using Eq. (34) and we get $z = 1/(2\bar{T}^2)+O(\bar{T}^{-4})$. Using the asymptotic expansion $-\mathrm{Li}_3(-z) = z+O(z^2)$, we finally find

$$Q(\bar{T}\to\infty,\eta=0) = \tfrac{1}{2}(3\pi-8) \approx 0.712\,389. \tag{B8}$$

This asymptotic limit is shown in Fig. 5(e) as a red dashed line and is in agreement with the numerical result.

APPENDIX C: MATRIX ELEMENTS OF THE EVOLUTION MATRIX IN THE MONOPOLE BASIS

The linear response analysis of the CBV equation using extended variational basis sets requires calculation of a large number of matrix elements. This task, however, can be simplified since the angular integrations appearing in expression for the matrix elements of M, Σ, and H_0 can be carried out analytically using the symmetries of the basis functions and the equilibrium state. The problem reduces to the evaluation of a 2D integral over $\bar{p}$ and $\bar{r}$ for each matrix element which can be done numerically accurately and efficiently.

In this Appendix, we provide readily computable formulas for the matrix elements in the monopole basis. We define the shorthands $R_\alpha \equiv 2m_\alpha+k_\alpha$, $P_\alpha \equiv 2n_\alpha+k_\alpha$ for given basis function ϕ_α. R_α and P_α count the powers of r and p appearing in ϕ_α, respectively.

1. Matrix elements of M

By definition, we have

$$\begin{aligned}\mathsf{M}_{\alpha\beta} &= \int d\bar{\Gamma}\,\Delta_0(\bar{p},\bar{r})\,\phi_\alpha\phi_\beta \\ &= \int (2\pi)\,\bar{r}\,d\bar{r}\,\frac{1}{(2\pi)^2}\,\bar{p}\,d\bar{p}\,\Delta_0(\bar{p},\bar{r})\,\bar{r}^{R_\alpha+R_\beta} \\ &\quad\times \bar{p}^{P_\alpha+P_\beta}\int_0^{2\pi}(\cos\psi)^{k_\alpha+k_\beta}\,d\psi \\ &= \frac{E(k_\alpha+k_\beta)(k_\alpha+k_\beta)!}{2^{k_\alpha+k_\beta}\left[\left(\frac{k_\alpha+k_\beta}{2}\right)!\right]^2}\Bigg[\int \bar{r}^{R_\alpha+R_\beta+1} \\ &\quad\times \bar{p}^{P_\alpha+P_\beta+1}\,\Delta_0(\bar{p},\bar{r})\,d\bar{r}\,d\bar{p}\Bigg],\end{aligned} \tag{C1}$$

where $E(n) = 1$ for even n and $E(n) = 0$ for odd n. For future reference, we define

$$h(n) = \frac{E(n)\,n!}{2^n\,[(n/2)!]^2} \tag{C2}$$

and

$$I_n^m[A(\bar{p},\bar{r})] = \int A(\bar{p},\bar{r})\,\bar{r}^{m+1}\,\bar{p}^{n+1}\,d\bar{r}\,d\bar{p}, \tag{C3}$$

using which we can write $\mathsf{M}_{\alpha\beta} = h(k_\alpha+k_\beta)\,I^{(R_\alpha+R_\beta)}_{(P_\alpha+P_\beta)}[\Delta_0]$.

2. Matrix elements of H_0

First, we evaluate the Poisson bracket $\{\phi_\beta,\bar{\mathcal{H}}_0\}$:

$$\begin{aligned}\{\phi_\beta,\bar{\mathcal{H}}_0\} &= \nabla_{\bar{\mathbf{r}}}\phi_\beta\cdot\nabla_{\bar{\mathbf{p}}}\bar{\mathcal{H}}_0 - \nabla_{\bar{\mathbf{p}}}\phi_\beta\cdot\nabla_{\bar{\mathbf{r}}}\bar{\mathcal{H}}_0 \\ &= \gamma_p\,(\bar{\mathbf{p}}\cdot\nabla_{\bar{\mathbf{r}}})\phi_\beta - \gamma_r\,(\bar{\mathbf{r}}\cdot\nabla_{\bar{\mathbf{p}}})\phi_\beta \\ &= \gamma_p[2m_\beta\,\phi_{(m_\beta-1,n_\beta,k_\beta+1)} + k_\beta\,\phi_{(m_\beta,n_\beta+1,k_\beta-1)}] \\ &\quad - \gamma_r[2n_\beta\,\phi_{(m_\beta,n_\beta-1,k_\beta+1)} - k_\beta\,\phi_{(m_\beta+1,n_\beta,k_\beta-1)}],\end{aligned} \tag{C4}$$

where

$$\gamma_r \equiv \bar{r}^{-2}\bar{\mathbf{r}}\cdot\nabla_{\bar{\mathbf{r}}}\bar{\mathcal{H}}_0 = 1+\bar{r}^{-2}\bar{\mathbf{r}}\cdot\nabla_{\bar{\mathbf{r}}}\bar{\Sigma}_0,$$
$$\gamma_p \equiv \bar{p}^{-2}\bar{\mathbf{p}}\cdot\nabla_{\bar{\mathbf{p}}}\bar{\mathcal{H}}_0 = 1+\bar{p}^{-2}\bar{\mathbf{p}}\cdot\nabla_{\bar{\mathbf{p}}}\bar{\Sigma}_0. \tag{C5}$$

Plugging Eq. (C4) into the definition of $(\mathsf{H}_0)_{\alpha\beta}$, we get

$$\begin{aligned}(\mathsf{H}_0)_{\alpha\beta} &= \int d\bar{\Gamma}\,\Delta_0\,\phi_\alpha\{\phi_\beta,\mathcal{H}_0\}\\ &= [2m_\beta\,h(k_\alpha+k_\beta+1)+k_\beta\,h(k_\alpha+k_\beta-1)]\\ &\quad\times I^{(R_\alpha+R_\beta-1)}_{(P_\alpha+P_\beta+1)}[\gamma_p\Delta_0]\\ &\quad-[2n_\beta\,h(k_\alpha+k_\beta+1)+k_\beta\,h(k_\alpha+k_\beta-1)]\\ &\quad\times I^{(R_\alpha+R_\beta+1)}_{(P_\alpha+P_\beta-1)}[\gamma_r\Delta_0].\end{aligned} \tag{C6}$$

3. Matrix elements of Σ

By definition,

$$\bar{\Sigma}[\Delta_0\phi_\beta] = \lambda_d\int\frac{d^2\bar{\mathbf{p}}'}{(2\pi)^2}\,u(|\bar{\mathbf{p}}-\bar{\mathbf{p}}'|,\eta)\,\Delta_0(\bar{p}',\bar{r})\,\phi_\beta(\bar{\mathbf{p}}',\bar{\mathbf{r}}). \tag{C7}$$

It is easy to verify that a simultaneous rotation of $\bar{\mathbf{r}}$ and $\bar{\mathbf{p}}$ leaves $\bar{\Sigma}[\Delta_0\phi_\beta]$ invariant, so that $\bar{\Sigma}[\Delta_0\phi_\beta]$ may only depend on $\bar{r}$, $\bar{p}$, and ϕ, the angle between $\bar{\mathbf{r}}$ and $\bar{\mathbf{p}}$. Let $\cos\psi = (\bar{\mathbf{p}}\cdot\bar{\mathbf{p}}')/(\bar{p}\bar{p}')$ and $\cos\phi = (\bar{\mathbf{r}}\cdot\bar{\mathbf{p}})/(\bar{r}\bar{p})$, so that $\bar{\mathbf{r}}\cdot\bar{\mathbf{p}}' = \bar{r}\bar{p}'\cos(\phi+\psi)$. Expanding $u(|\bar{\mathbf{p}}-\bar{\mathbf{p}}'|,\eta)$ in a cosine series,

$$u(|\bar{\mathbf{p}}-\bar{\mathbf{p}}'|,\eta) = \sum_{n=0}^{\infty}u^{(n)}(\bar{p},\bar{p}';\eta)\cos(n\psi), \tag{C8}$$

where

$$\begin{aligned}u^{(n)}(\bar{p},\bar{p}') &= \frac{1}{\pi(\delta_{n,0}+1)}\\ &\quad\times\int_0^{2\pi}d\psi\,u(\sqrt{\bar{p}^2+\bar{p}'^2-2\bar{p}\bar{p}'\cos\psi},\eta)\cos n\psi,\end{aligned} \tag{C9}$$

and plugging into Eq. (C7), we get

$$\begin{aligned}&\bar{\Sigma}[\Delta_0\phi_\beta](\bar{p},\bar{r},\phi)\\ &\quad=\lambda_d\int\frac{\bar{p}'\,d\bar{p}'}{2\pi}\,\Delta_0(\bar{p}',\bar{r})\,\bar{p}'^{P_\beta}\bar{r}^{R_\beta}\\ &\quad\times\sum_{n=0}^{\infty}u(\bar{p},\bar{p}';\eta)\int_0^{2\pi}\frac{d\psi}{2\pi}\,\cos(n\psi)\cos(\phi+\psi)^{k_\beta}.\end{aligned} \tag{C10}$$

The angular integration can be evaluated using contour integral techniques:

$$\begin{aligned}&\int_0^{2\pi}\frac{d\psi}{2\pi}\,\cos(n\psi)\cos(\phi+\psi)^k\\ &\quad=\left[\frac{k!}{2^k}\frac{\theta(k-n)\,E(k+n)}{\left[\left(\frac{k-n}{2}\right)!\right]\left[\left(\frac{k+n}{2}\right)!\right]}\right]\cos(n\phi),\end{aligned} \tag{C11}$$

where $\theta(n)=1$ if $n\geqslant 0$ and $\theta(n)=0$ otherwise. We denote the numerical prefactor in the brackets of the above equation by $g(n,k)$. Plugging this into Eq. (C10), we get

$$\bar{\Sigma}[\Delta_0\phi_\beta](\bar{p},\bar{r},\phi) = \lambda_d\sum_{n=0}^{k_\beta}Q^{(n)}_\beta(\bar{p},\bar{r})\cos(n\phi), \tag{C12}$$

where

$$\begin{aligned}Q^{(n)}_\beta(\bar{p},\bar{r}) &= -g(n,k_\beta)\,\bar{r}^{R_\beta}\int\frac{d\bar{p}'}{2\pi}\,\Delta_0(\bar{p}',\bar{r})\,\bar{p}'^{(P_\beta+1)}\\ &\quad\times u^{(n)}(\bar{p},\bar{p}';\eta).\end{aligned} \tag{C13}$$

The last integral can be easily evaluated numerically. Also, note that we only need $u^{(n)}$ up to $n=k_\beta$ in order to evaluate $\bar{\Sigma}[\Delta_0\phi_\beta]$ exactly. This is due to the fact that $g(n,k_\beta)$ vanishes for $n>k_\beta$. Having evaluated $\bar{\Sigma}[\Delta_0\phi_\beta]$, $\Sigma_{\alpha\beta}$ can be evaluated readily by appealing to its definition:

$$\begin{aligned}\Sigma_{\alpha\beta} &= \lambda_d\sum_{n=0}^{k_\beta}\big([2m_\alpha\,g(n,k_\alpha+1)+k_\alpha\,g(n,k_\alpha-1)]\\ &\quad\times I^{(R_\alpha-1)}_{(P_\alpha+1)}\big[Q^{(n)}_\beta\Delta_0\gamma_p\big]-[2n_\alpha\,g(n,k_\alpha+1)\end{aligned} \tag{C14}$$

$$+k_\alpha\,g(n,k_\alpha-1)]\,I^{(R_\alpha+1)}_{(P_\alpha-1)}\big[Q^{(n)}_\beta\Delta_0\gamma_r\big]\big). \tag{C15}$$

4. Matrix elements of I_c

The evaluation of the matrix elements of the linearized collision integral operator is the most computationally expensive part of the calculation. Once HF self-energy corrections are taken into account, deviation of quasiparticle dispersion from the bare quadratic dispersion makes the calculations even more challenging. The collision integrals are commonly evaluated with bare quadratic dispersions. This is justified in the Boltzmann equation limit, where mean-field corrections are neglected altogether. Here, since we have included mean-field effects on the dynamics, we must also use the dressed quasiparticles dispersion in order to satisfy conservation of energy. In order to do this in a numerically tractable way, we have found that the quasiparticle dispersions can be approximated well using a local effective mass approximation (LEMA) within an error of less than 2%. To this end, we approximate the dressed quasiparticle energies as

$$\bar{\mathcal{H}}_0(\bar{p},\bar{r}) \approx \varepsilon_0(\bar{r}) + \frac{\bar{p}^2}{2m^*(r)} + \frac{\bar{r}^2}{2}, \tag{C16}$$

where

$$\begin{aligned}\varepsilon_0(\bar{r}) &= \bar{\Sigma}_0(\bar{r};0),\\ m^*(\bar{r}) &= \left[1+\partial^2_{\bar{p}}\,\bar{\Sigma}_0(\bar{r};\bar{p})\big|_{\bar{p}=0}\right]^{-1}.\end{aligned} \tag{C17}$$

As we will see shortly, this approximation allows us to put the collision integral into a simple form suitable for numerical treatments. As a first step, we go to the center-of-mass frame of the colliding particles and define

$$\begin{aligned}\bar{\mathbf{p}} &= \frac{\bar{\mathbf{P}}}{2}+\bar{\mathbf{q}},\quad \bar{\mathbf{p}}_1 = \frac{\bar{\mathbf{P}}}{2}-\bar{\mathbf{q}},\\ \bar{\mathbf{p}}' &= \frac{\bar{\mathbf{P}}'}{2}+\bar{\mathbf{q}}',\quad \bar{\mathbf{p}}'_1 = \frac{\bar{\mathbf{P}}'}{2}-\bar{\mathbf{q}}',\end{aligned} \tag{C18}$$

using which we get

$$d^2\bar{\mathbf{r}}\,\frac{d^2\bar{\mathbf{p}}}{(2\pi)^2}\,\frac{d^2\bar{\mathbf{p}}_1}{(2\pi)^2}\,\frac{d^2\bar{\mathbf{p}}'}{(2\pi)^2}\,\frac{d^2\bar{\mathbf{p}}'_1}{(2\pi)^2}\,(2\pi)\delta(\Delta\bar{E})\,(2\pi)^2\delta(\Delta\bar{\mathbf{P}}) \to \frac{m^*(\bar{r})}{2}\,\bar{r}\,d\bar{r}\,d\psi\,\frac{\bar{P}\,d\bar{P}}{2\pi}\,\frac{\bar{q}\,d\bar{q}}{2\pi}\,\frac{d\phi}{2\pi}\,\frac{d\phi'}{2\pi}, \tag{C19}$$

where ϕ, ϕ', and ψ are defined as $\cos\phi = \bar{\mathbf{q}}\cdot\bar{\mathbf{P}}/(\bar{q}\bar{P})$, $\cos\phi' = \bar{\mathbf{q}}'\cdot\bar{\mathbf{P}}/(\bar{q}'\bar{P})$, and $\cos\psi = \bar{\mathbf{r}}\cdot\bar{\mathbf{P}}/(\bar{r}\bar{P})$. Note that $\bar{\mathbf{P}} \equiv \bar{\mathbf{P}}'$ and $\bar{q} \equiv \bar{q}'$ in the rest of the integrand due to conservation of momentum and energy. The scattering amplitude $\bar{\mathcal{M}} = \lambda_d[u(|\bar{\mathbf{p}}-\bar{\mathbf{p}}'|,\eta) - u(|\bar{\mathbf{p}}-\bar{\mathbf{p}}'_1|,\eta)] \to \lambda_d[u(2\bar{q}|\sin[(\phi-\phi')/2]|,\eta) - u(2\bar{q}|\cos[(\phi-\phi')/2]|,\eta)]$. The product of the equilibrium distribution functions, $n_0\,n_{0,1}(1-n'_0)(1-n'_{0,1})$ can be conveniently written as

$$n_0\,n_{0,1}(1-n'_0)(1-n'_{0,1}) \to \frac{1}{4}\,\frac{1}{\cosh E + \cosh\gamma}\,\frac{1}{\cosh E + \cosh\gamma'},$$

where $E = \bar{\beta}(\bar{P}^2/4 + \bar{q}^2)/[2m^*(\bar{r})] + \bar{\beta}\bar{r}^2/2 - \bar{\beta}\bar{\mu}$, $\gamma = \bar{\beta}\bar{P}\bar{q}\cos\phi/[2m^*(\bar{r})]$, and $\gamma' = \bar{\beta}\bar{P}\bar{q}\cos\phi'/[2m^*(\bar{r})]$. The angle ψ is only present in $\mathrm{S}[\phi_\alpha]\mathrm{S}[\phi_\alpha]$. Therefore, the integration over ψ is immediate and elementary, which we evaluate using MATHEMATICA and define $\mathrm{S}_{\alpha\beta}(\bar{r},\bar{P},\bar{q},\phi,\phi') \equiv \int d\psi\,\mathrm{S}[\phi_\alpha]\mathrm{S}[\phi_\beta]$. The integral can be put in a more useful form using a spherical change of variables, $\bar{P} = (8\rho/\bar{\beta})^{1/2}\sin\xi\,\cos\nu$, $\bar{q} = (2\rho/\bar{\beta})^{1/2}\sin\xi\,\sin\nu$ and $\bar{r} = (2\rho/\beta)^{1/2}\cos\xi$, where $\rho\in[0,\infty)$, $\nu\in[0,\pi/2]$, and $\xi\in[0,\pi/2]$. The final expression is

$$\begin{aligned}\mathscr{I}_{\alpha\beta} = &-\frac{(2N)^{\frac{1}{2}}\lambda_d^2}{8(2\pi)^2\,\bar{\beta}^{N_\alpha+N_\beta+3}}\int_0^\infty \rho^2\,d\rho\int_0^{2\pi}\frac{d\phi}{2\pi}\int_0^{2\pi}\frac{d\phi'}{2\pi}\int_0^{\frac{\pi}{2}}d\xi\,\sin^3\xi\,\cos\xi\int_0^{\frac{\pi}{2}}d\nu\,\sin 2\nu\\ &\times \mathrm{S}_{\alpha\beta}(\sqrt{2\rho}\cos\xi,\sqrt{8\rho}\sin\xi\,\cos\nu,\sqrt{2\rho}\sin\xi\,\sin\nu,\phi,\phi')\,m^*(\bar{r})\\ &\times\left[\sqrt{\bar{\beta}}\,u\big(2\sqrt{2\rho/\bar{\beta}}\,\sin\xi\,\sin\nu\,|\sin[(\phi-\phi')/2]|,\eta\big) - \sqrt{\bar{\beta}}\,u\big(2\sqrt{2\rho/\bar{\beta}}\,\sin\xi\,\sin\nu\,|\cos[(\phi-\phi')/2]|,\eta\big)\right]^2\\ &\times\{[\cosh(\rho\sin^2\xi/m^*(\bar{r}) + \rho\cos^2\xi + \bar{\beta}\varepsilon_0(\bar{r}) - \bar{\beta}\bar{\mu}) + \cosh(\rho\,\sin^2\xi\sin 2\nu\cos\phi/m^*(\bar{r}))]\times(\phi\leftrightarrow\phi')\}^{-1},\end{aligned} \tag{C20}$$

where $N_{a(b)} = m_{a(b)} + n_{a(b)} + k_{a(b)}$ and $\bar{r} \equiv \sqrt{2\rho/\bar{\beta}}\cos\xi$ in $m^*(\bar{r})$ and $\varepsilon(\bar{r})$. We evaluate the above 5D integral for all pairwise combination of basis functions using a numerical Monte Carlo integration with 5×10^8 points, which we found to yield a relative statistical error of less than 10^{-3} in all cases.

APPENDIX D: MATRIX ELEMENTS OF THE EVOLUTION MATRIX IN THE QUADRUPOLE BASIS

In this Appendix, we provide readily computable expressions for various matrix elements in the quadrupole basis by carrying out the angular integrations analytically. For a given quadrupole basis function $\xi_i\phi_\alpha$, we define the shorthand (μ_i,ν_i) as the number of powers of r and p present in ξ_i, respectively, that is, $(\mu_1,\nu_1) = (2,0)$, $(\mu_2,\nu_2) = (1,1)$, and $(\mu_3,\nu_3) = (0,2)$.

1. Matrix elements of M

The angular integrations in M can be easily carried out using the parametrization $\cos\phi = \hat{\mathbf{r}}\cdot\hat{x}$ and $\cos\psi = \bar{\mathbf{r}}\cdot\bar{\mathbf{p}}/(\bar{r}\bar{p})$. In this variables, we get $\xi_i = \bar{r}^{\mu_i}\bar{p}^{\nu_i}\cos(2\phi+\nu_j\psi)$. The angular integration are elementary and we find

$$\mathsf{M}^{ij}_{\alpha\beta} = \int d\bar{\Gamma}\,\Delta_0\,\xi_i\,\xi_j\,\phi_\alpha\phi_\beta = \frac{1}{2}\,g(|\nu_i-\nu_j|,k_\alpha+k_\beta)\,I^{(R_\alpha+R_\beta+\mu_i+\mu_j)}_{(P_\alpha+P_\beta+\nu_i+\nu_j)}[\Delta_0]. \tag{D1}$$

2. Matrix elements of H

As a first step, we evaluate the Poisson bracket $\{\xi_j\phi_\beta,\bar{\mathcal{H}}_0\} = \xi_j\{\phi_\beta,\bar{\mathcal{H}}_0\} + \phi_\beta\{\xi_j,\bar{\mathcal{H}}_0\}$. The expression for $\{\phi_\beta,\bar{\mathcal{H}}_0\}$ is known from the previous Appendix [Eq. (C4)]. We can write $\{\xi_j,\bar{\mathcal{H}}_0\} = X_{jk}(\bar{p},\bar{r})\,\xi_k$ (sum over k is implied), where

$$X_{jk} = \begin{pmatrix} 0 & 2\gamma_p & 0\\ -\gamma_r & 0 & \gamma_p\\ 0 & -2\gamma_r & 0\end{pmatrix}. \tag{D2}$$

Therefore, we get

$$\begin{aligned}(\mathsf{H}_0)^{ij}_{\alpha\beta} &= \int d\bar{\Gamma}\,\Delta_0\,\xi_i\,\phi_\alpha\{\xi_j\phi_\beta,\bar{\mathcal{H}}_0\}\\ &= \underbrace{\int d\bar{\Gamma}\,\Delta_0\,\phi_\alpha\{\phi_\beta,\bar{\mathcal{H}}_0\}\,\xi_i\xi_j}_{(\mathsf{H}_0)^{ij}_{\alpha\beta,1}} + \underbrace{\int d\bar{\Gamma}\,\Delta_0\,\phi_\alpha\phi_\beta\,X_{jk}\,\xi_i\,\xi_k}_{(\mathsf{H}_0)^{ij}_{\alpha\beta,2}}.\end{aligned} \tag{D3}$$

The angular integrations in $(\mathsf{H}_0)^{ij}_{\alpha\beta,1}$ can be most easily evaluated using the parametrization defined earlier, $\cos\phi = \hat{\mathbf{r}}\cdot\hat{x}$ and $\cos\psi = \bar{\mathbf{r}}\cdot\bar{\mathbf{p}}/(\bar{r}\bar{p})$. The final result is

$$\begin{aligned}(\mathsf{H}_0)^{ij}_{\alpha\beta,1} = &\tfrac{1}{2}[2m_\beta\,g(|\nu_i-\nu_j|,k_\alpha+k_\beta+1)\\ &+k_\beta\,g(|\nu_i-\nu_j|,k_\alpha+k_\beta-1)]\,I^{(R_\alpha+R_\beta+\mu_i+\mu_j-1)}_{(P_\alpha+P_\beta+\nu_i+\nu_j+1)}\\ &\times[\Delta_0\,\gamma_p] - \tfrac{1}{2}[2n_\beta\,g(|\nu_i-\nu_j|,k_\alpha+k_\beta+1)\\ &+k_\beta\,g(|\nu_i-\nu_j|,k_\alpha+k_\beta-1)]\\ &\times I^{(R_\alpha+R_\beta+\mu_i+\mu_j+1)}_{(P_\alpha+P_\beta+\nu_i+\nu_j-1)}[\Delta_0\,\gamma_r].\end{aligned}$$

The angular integrations in $(\mathsf{H}_0)^{ij}_{\alpha\beta,2}$ are similar to those in $(\mathsf{M})^{ij}_{\alpha\beta}$ and the result is

$$(\mathsf{H}_0)^{ij}_{\alpha\beta,2} = \tfrac{1}{2}\, g(|\nu_i - \nu_k|, k_\alpha + k_\beta) I^{(R_\alpha+R_\beta+\mu_i+\mu_k)}_{(P_\alpha+P_\beta+\nu_i+\nu_k)}[\Delta_0\, X_{jk}]. \tag{D4}$$

3. Matrix elements of Σ

Similar to the monopole case, the first step is evaluating $\bar{\Sigma}[\Delta_0 \xi_j \phi_\beta]$:

$$\begin{aligned}\bar{\Sigma}&[\Delta_0 \xi_j \phi_\beta] \\ &= \lambda_d \int \frac{\bar{p}'\, d\bar{p}'}{2\pi} \sum_{n=0}^{\infty} u^{(n)}(\bar{p}, \bar{p}'; \eta)\, \Delta_0(\bar{p}', \bar{r})\, \bar{r}^{R_\beta+\mu_j}\, \bar{p}'^{P_\beta+\nu_j} \\ &\quad \times \int \frac{d\psi'}{2\pi} \cos^{k_\beta}(\psi + \psi')\, \cos[2\phi + \nu_j(\psi + \psi')] \\ &\quad \times \cos(n\psi'),\end{aligned} \tag{D5}$$

where we have expressed $u(|\bar{\mathbf{p}} - \bar{\mathbf{p}}'|, \eta)$ as a cosine series like before. The ψ' integration can be conveniently carried out using the contour integral technique and gives $\tilde{g}(\nu_j, n, k_\beta) \cos(2\phi) \cos(n\psi) - \tilde{h}(\nu_j, n, k_\beta) \sin(2\phi) \sin(n\psi)$, where

$$\begin{aligned}\tilde{g}(0,n,k) &\equiv g(n,k), \\ \tilde{g}(1,n,k) &\equiv g(n,k+1), \\ \tilde{g}(2,n,k) &\equiv 2g(n,k+2) - g(n,k), \\ \tilde{h}(\nu,n,k) &\equiv \tilde{g}(\nu,n,k) - g(\nu+n,k).\end{aligned} \tag{D6}$$

Plugging this back into Eq. (D5), we get

$$\begin{aligned}\bar{\Sigma}[\Delta_0 \xi_j \phi_\beta] = \sum_{n=0}^{k_\beta+2} &Q^{(n)}_{\beta,j}(\bar{p}, \bar{r}) [\tilde{g}(\nu_j, n, k_\beta) \cos(2\phi) \\ &\times \cos(n\psi) - \tilde{h}(\nu_j, n, k_\beta) \sin(2\phi) \sin(n\psi)],\end{aligned} \tag{D7}$$

where

$$\begin{aligned}Q^{(n)}_{\beta,j}(\bar{p}, \bar{r}) = \lambda_d \int \frac{d\bar{p}'}{2\pi}\, &\bar{r}^{R_\beta+\mu_j}\, \bar{p}'^{P_\beta+\nu_j+1} \\ &\times u(\bar{p}, \bar{p}'; \eta)\, \Delta_0(\bar{p}', \bar{r}).\end{aligned} \tag{D8}$$

The last integral can be evaluated easily numerically. The final result can be expressed easily using using last two expressions:

$$\begin{aligned}(\Sigma)^{ij}_{\alpha\beta} = \sum_{n=0}^{k_\beta+2} \Bigg[&\frac{1}{2}\, G^{(\nu_k,n,k_\alpha)}_{(\nu_j,n,k_\beta)}\, I^{(R_\alpha+\mu_k)}_{(P_\alpha+\nu_k)} \big[\Delta_0 Q^{(n)}_{\beta,j} X_{ik}\big] \\ &+ \frac{1}{2}\big(2m_\alpha\, G^{(\nu_i,n,k_\alpha+1)}_{(\nu_j,n,k_\beta)} + k_\alpha\, G^{(\nu_i,n,k_\alpha-1)}_{(\nu_j,n,k_\beta)}\big) \\ &\times I^{(R_\alpha+\mu_i-1)}_{(P_\alpha+\nu_i+1)} \big[\Delta_0 Q^{(n)}_{\beta,j} \gamma_p\big] \\ &+ \frac{1}{2}\big(2n_\alpha\, G^{(\nu_i,n,k_\alpha+1)}_{(\nu_j,n,k_\beta)} + k_\alpha\, G^{(\nu_i,n,k_\alpha-1)}_{(\nu_j,n,k_\beta)}\big) \\ &\times I^{(R_\alpha+\mu_i+1)}_{(P_\alpha+\nu_i-1)} \big[\Delta_0 Q^{(n)}_{\beta,j} \gamma_r\big]\Bigg],\end{aligned} \tag{D9}$$

where we have defined the shorthand notation $G^{(\nu_1,n_1,k_1)}_{(\nu_2,n_2,k_2)} = \tilde{g}(\nu_1,n_1,k_1)\, \tilde{g}(\nu_2,n_2,k_2) + \tilde{h}(\nu_1,n_1,k_1)\, \tilde{h}(\nu_2,n_2,k_2)$.

4. Matrix elements of I_c

The matrix elements of the collision integral in the quadrupole basis is identical in form to those of the monopole basis [Eq. (C20)]. The only differences are (1) $\mathsf{S}_{\alpha\beta}$ must be replaced with

$$\mathsf{S}^{ij}_{\alpha\beta}(\bar{r}, \bar{P}, \bar{q}, \phi, \phi') \equiv \int \frac{d\theta}{2\pi} d\psi\, \mathrm{S}[\xi_i \phi_\alpha]\, \mathrm{S}[\xi_j \phi_\beta], \tag{D10}$$

where we introduced an extra angle $\cos\theta = \mathbf{e}_x \cdot \bar{\mathbf{P}}/\bar{P}$, and (2) the prefactor $\bar{\beta}^{N_\alpha+N_\beta+3} \to \bar{\beta}^{N_\alpha+N_\beta+5}$ in the denominator due to the extra powers of $\bar{\beta}^{-1}$ introduced by ξ_i and ξ_j. The definition of $N_{\alpha(\beta)}$ is the same as before.

APPENDIX E: CALCULATION OF THE COLLISION INTEGRALS WITH EXACT HARTREE-FOCK QUASIPARTICLE DISPERSIONS

In Appendix C4, we simplified the expression for the collision integral matrix elements using the LEMA. Although we found this scheme to be a decent approximation in the weakly interacting regime (the approximate dispersions lie within a few percents of the exact HF dispersions), one may argue that an exact treatment is necessary for stronger interactions. In particular, this may have important consequences when one is looking at the effects that crucially depend on self-energy corrections, such as the damping of the nodeless monopole mode. In this section, we discuss this issue and present numerical justification for the reliability of LEMA.

The major simplification resulting from LEMA is the possibility of an analytic treatment of the δ function in the collision integral associated to the conservation of energy [see Eq. (C19)]. In that case, LEMA simply yields $q = q'$, where q and q' are the magnitude of the momenta of the initial and final scattering pairs in the center-of-mass frame. Without a (local) quadratic dispersion, this simple result does not hold anymore and, in general, there is no easy way of treating the

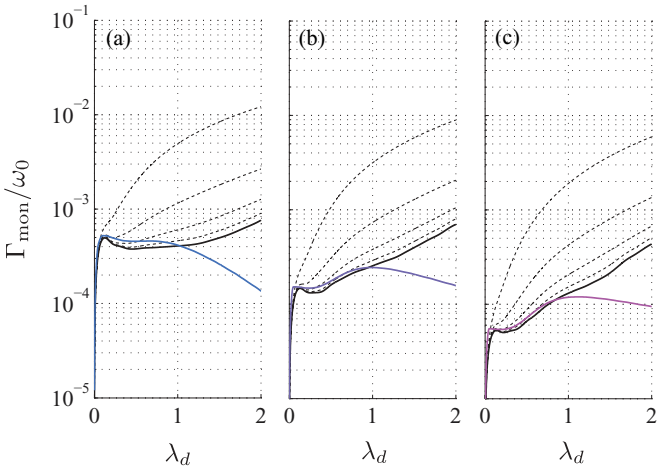

FIG. 15. (Color online) The damping rate of the monopole oscillations in 2D and with $N = 2200$ particles. (a) $T/T_F = 0.5$, (b) $T/T_F = 1.0$, and (c) $T/T_F = 1.5$. The (light) solid colored lines are the previously discussed result obtained using the LEMA. The dashed lines denote approximate solutions obtained by relaxing the conservation of energy (from top to bottom, $\sigma = 0.05$, 0.02, 0.01, and 0.005). The solid black line is the extrapolation to $\sigma = 0$ (the exact result).

δ function analytically since the quasiparticle dispersions are evaluated numerically. Here, we introduce a simple numerical approach to overcome this difficulty. Using a limiting process to to define the δ functions,

$$\delta(\Delta\bar{E}) = \lim_{\sigma\to 0} \frac{1}{\sqrt{2\pi}\sigma} e^{-\Delta\bar{E}^2/(2\sigma^2)}, \tag{E1}$$

we replace the δ function with Gaussians and calculate the collision integrals for various values of σ. We find the $\sigma \to 0$ limit by extrapolation. This approach is considerably more computationally demanding than LEMA; however, it yields an accurate calculation of the collision integral matrix elements. The integrals are 6D in this case (the variables being $\bar{r}$, $\bar{P}$, $\bar{q}$, $\bar{q}'$, ϕ, and ϕ') since q and q' may assume different values now.

We implemented the above method for both monopole and quadrupole oscillations within a second-order basis set. The extrapolation is carried out using a polynomial fit. Figure 15 shows the damping of monopole oscillations obtained using several choices of σ, the extrapolated result, and the LEMA result for reference. The matching between the effective mass approximation and the exact result is excellent up to $\lambda_d \sim 1$. The LEMA result, however, deviates from the exact result for $\lambda_d \gtrsim 1$. Nonetheless, we find $\gamma_{\rm mon}^{\rm exact} < 10^{-3}\omega_0$ and our conclusion about the smallness of the damping of the nodeless monopole mode remains valid. Finally, we note that the beyond-LEMA refinement to the prediction for the frequency of monopole oscillations is much smaller (a relative correction of about 10^{-6}). This is due to the fact that the frequency shift essentially results from the self-energy corrections on the dynamical side of the CBV equation which is already treated exactly.

[1] M. A. Baranov, Phys. Rep. **464**, 71 (2008).
[2] T. Lahaye, C. Menotti, L. Santos, M. Lewenstein, and T. Pfau, Rep. Prog. Phys. **72**, 126401 (2009).
[3] M. Lu, N. Q. Burdick, S. H. Youn, and B. L. Lev, Phys. Rev. Lett. **107**, 190401 (2011).
[4] K. Aikawa, A. Frisch, M. Mark, S. Baier, A. Rietzler, R. Grimm, and F. Ferlaino, Phys. Rev. Lett. **108**, 210401 (2012).
[5] K.-K. Ni *et al.*, Science **322**, 231 (2008); Nature (London) **464**, 1324 (2010); M. H. G. de Miranda *et al.*, Nat. Phys. **7**, 502 (2011).
[6] J. M. Sage, S. Sainis, T. Bergeman, and D. DeMille, Phys. Rev. Lett. **94**, 203001 (2005).
[7] J. Deiglmayr, M. Repp, A. Grochola, O. Dulieu, R. Wester, and M. Weidemüller, J. Phys.: Conf. Ser. **264**, 012014 (2011).
[8] M. Lu, N. Q. Burdick, and B. L. Lev, Phys. Rev. Lett. **108**, 215301 (2012).
[9] A. Altmeyer, S. Riedl, C. Kohstall, M. J. Wright, R. Geursen, M. Bartenstein, C. Chin, J. H. Denschlag, and R. Grimm, Phys. Rev. Lett. **98**, 040401 (2007).
[10] C. Cao *et al.*, Science **331**, 58 (2010).
[11] P. K. Kovtun, D. T. Son, and A. O. Starinets, Phys. Rev. Lett. **94**, 111601 (2005).
[12] F. Dalfovo, S. Giorgini, L. P. Pitaevskii, and S. Stringari, Rev. Mod. Phys. **71**, 463 (1999).
[13] R. Grimm, in *Proceedings of the International School of Physics "Enrico Fermi"*, Ultra-cold Fermi Gases, edited by M. Inguscio, W. Ketterle, and C. Salomon, Vol. 164 (IOS Press, Amsterdam, 2007).
[14] E. Vogt, M. Feld, B. Fröhlich, D. Pertot, M. Koschorreck, and M. Köhl, Phys. Rev. Lett. **108**, 070404 (2012).
[15] T. Schäfer, Phys. Rev. A **85**, 033623 (2012).
[16] E. Taylor and M. Randeria, Phys. Rev. Lett. **109**, 135301 (2012).
[17] T. Enss, C. Küppersbusch, and L. Fritz, Phys. Rev. A **86**, 013617 (2012).
[18] L. Wu and Y. Zhang, Phys. Rev. A **85**, 045601 (2012).
[19] L. P. Kadanoff, G. Baym, and D. Pines, *Quantum Statistical Mechanics* (Westview Press, Boulder, CO, 1994).
[20] E. M. Lifshitz and L. P. Pitaevskii, "*Physical Kinetics*", *Course of Theoretical Physics*, Vol. 10 (Butterworth-Heinemann, 1981).
[21] There are exceptional cases where certain dynamical symmetries forbid collisions; see Ref. [14], for example.
[22] K. Goral, B.-G. Englert, and K. Rzazewski, Phys. Rev. A **63**, 033606 (2001).
[23] K. Góral, M. Brewczyk, and K. Rzazewski, Phys. Rev. A **67**, 025601 (2003).
[24] A. R. P. Lima and A. Pelster, Phys. Rev. A **81**, 021606(R) (2010).
[25] A. R. P. Lima and A. Pelster, Phys. Rev. A **81**, 063629 (2010).
[26] T. Sogo, L. He, T. Miyakawam, S. Yi, H. Lu, and H. Pu, New J. Phys. **11**, 055017 (2009).
[27] M. Abad, A. Recati, and S. Stringari, Phys. Rev. A **85**, 033639 (2012).
[28] C. Ticknor, Phys. Rev. A **80**, 052702 (2009).
[29] F. Arnecke, H. Friedrich, and P. Raab, Phys. Rev. A **78**, 052711 (2008).
[30] Y. Castin and R. Dum, Phys. Rev. Lett. **77**, 5315 (1996); V. M. Perez-Garcia, H. Michinel, J. I. Cirac, M. Lewenstein, and P. Zoller, *ibid.* **77**, 5320 (1996); K. G. Singh and D. S. Rokhsar, *ibid.* **77**, 1667 (1996); F. Dalfovo, C. Minniti, S. Stringari, and L. Pitaevskii, Phys. Lett. A **227**, 259 (1997).
[31] L. Vichi, J. Low Temp. Phys. **121**, 177 (2000).
[32] L. Boltzmann, in *Wissenschaftliche Abhandlungen*, edited by F. Hasenorl, Vol. II (J. A. Barth, Leipzig, 1909), p. 83.
[33] A. Griffin, W.-C. Wu, and S. Stringari, Phys. Rev. Lett. **78**, 1838 (1997).
[34] S. Chiacchiera, T. Lepers, D. Davesne, and M. Urban, Phys. Rev. A **79**, 033613 (2009).
[35] S. Chiacchiera, T. Lepers, D. Davesne, and M. Urban, Phys. Rev. A **84**, 043634 (2011).
[36] P. Danielewics, Ann. Phys. **152**, 239 (1984).
[37] The non-normality of the linearized Boltzmann-Vlasov equation is the key to Landau damping [see N. G. van Kampen, Physica **21**, 949 (1955)]. However, as we argued earlier, dipole-dipole interactions are not long-ranged enough to give rise to this phenomenon.
[38] D. Guéry-Odelin, F. Zambelli, J. Dalibard, and S. Stringari, Phys. Rev. A **60**, 4851 (1999).
[39] D. S. Novikov, arXiv:cond-mat/0603184.
[40] M. Babadi and E. Demler, Phys. Rev. B **84**, 235124 (2011).
[41] P.-A. Pantel, D. Davesne, S. Chiacchiera, and M. Urban, Phys. Rev. A **86**, 023635 (2012).
[42] L. D. Landau and E. M. Lifshitz, "*Fluid Mechanics*" 2nd edn., *Course of Theoretical Physics*, Vol. 6 (Butterworth-Heinemann, 1987).
[43] M. Babadi and E. Demler, Phys. Rev. A **84**, 033636 (2011).